Nucleic Acids Research, 2024, **52**, 6424–6440
https://doi.org/10.1093/nar/gkae445
Advance access publication date: 27 May 2024
Genome Integrity, Repair and Replication

The TIMELESS and PARP1 interaction suppresses replication-associated DNA gap accumulation

Joanne Saldanha [1,2], Julie Rageul[1], Jinal A. Patel[1], Amy L. Phi[1], Natalie Lo[1], Jennifer J. Park[1] and Hyungjin Kim [1,2,3,*]

[1]Department of Pharmacological Sciences, State University of New York at Stony Brook, Stony Brook, NY 11794, USA
[2]The Graduate program in Genetics, State University of New York at Stony Brook, Stony Brook, NY 11794, USA
[3]Stony Brook Cancer Center, Renaissance School of Medicine at Stony Brook University, Stony Brook, NY 11794, USA
[*]To whom correspondence should be addressed. Tel: +1 631 444 3134; Fax: +1 631 444 9749; Email: hyungjin.kim@stonybrook.edu

Abstract

TIMELESS (TIM) in the fork protection complex acts as a scaffold of the replisome to prevent its uncoupling and ensure efficient DNA replication fork progression. Nevertheless, its underlying basis for coordinating leading and lagging strand synthesis to limit single-stranded DNA (ssDNA) exposure remains elusive. Here, we demonstrate that acute degradation of TIM at ongoing DNA replication forks induces the accumulation of ssDNA gaps stemming from defective Okazaki fragment (OF) processing. Cells devoid of TIM fail to support the poly(ADP-ribosyl)ation necessary for backing up the canonical OF processing mechanism mediated by LIG1 and FEN1. Consequently, recruitment of XRCC1, a known effector of PARP1-dependent single-strand break repair, to post-replicative ssDNA gaps behind replication forks is impaired. Physical disruption of the TIM–PARP1 complex phenocopies the rapid loss of TIM, indicating that the TIM–PARP1 interaction is critical for the activation of this compensatory pathway. Accordingly, combined deficiency of FEN1 and the TIM–PARP1 interaction leads to synergistic DNA damage and cytotoxicity. We propose that TIM is essential for the engagement of PARP1 to the replisome to coordinate lagging strand synthesis with replication fork progression. Our study identifies TIM as a synthetic lethal target of OF processing enzymes that can be exploited for cancer therapy.

Graphical abstract

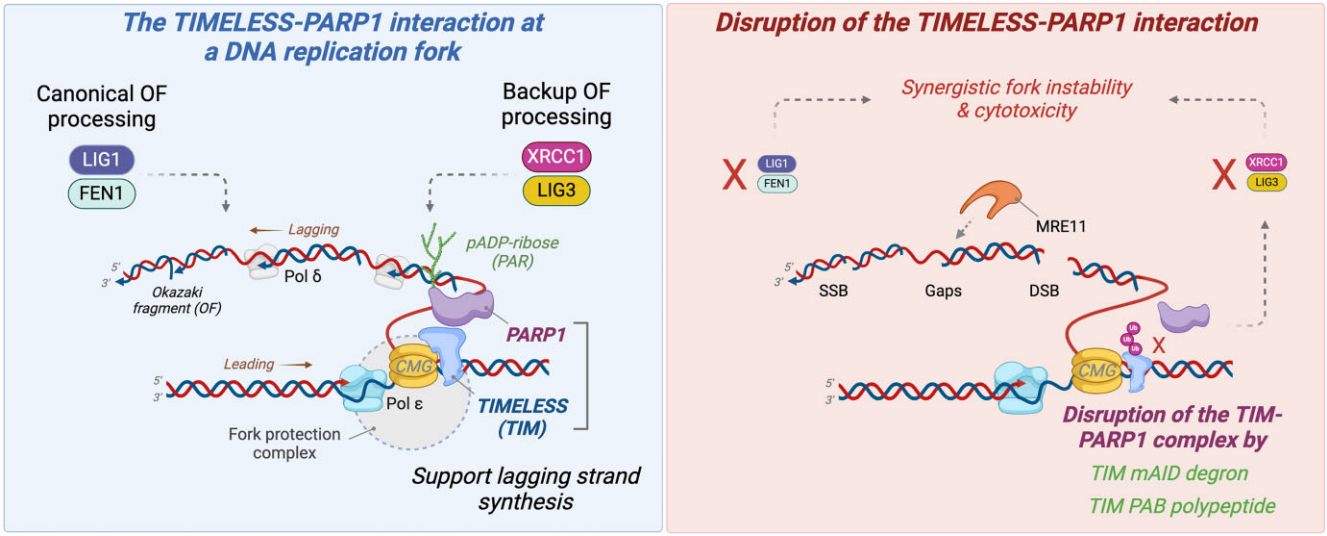

Introduction

DNA replication is achieved by the coordinated action of the replisome that couples the unwinding activity of the CDC45/MCM2-7/GINS (CMG) helicase complex and incorporation of nucleotides complementary to a DNA template by replicative polymerases (1). The fork protection complex (FPC), which consists of TIMELESS (TIM), TIPIN, CLASPIN and AND-1 in mammalian cells, plays a key role in maintaining the integrity of the replisome and coupling its activity, thus enabling efficient replication fork progression (2). The TIM-TIPIN heterodimer (Tof1-Csm3 in *Saccharomyces cerevisiae*) grips double-stranded DNA (dsDNA) in front of the CMG to stabilize the association of the replisome to DNA and facilitate strand separation (3,4). This unique

Received: January 3, 2024. **Revised:** April 9, 2024. **Editorial Decision:** May 2, 2024. **Accepted:** May 10, 2024

positioning of TIM ahead of the replisome is thought to be necessary to pause replication under replication stress (5). CLASPIN/Mrc1, which makes extensive contacts with other components within the replisome, is sufficient to drive replication fork progression *in vitro*, while maximal fork elongation is achieved by the addition of the TIM-TIPIN complex, further highlighting the role of TIM in supporting DNA replication (6,7). AND-1/Ctf4 bridges polymerase (Pol) α to the CMG to promote the initiation of DNA replication at origins of replication (8,9). Furthermore, TIM-TIPIN directly interacts with replication protein A (RPA), a single-stranded DNA (ssDNA)-binding protein complex, at stalled forks to facilitate ATR-dependent CHK1 phosphorylation and propagate the DNA damage checkpoint in response to replication stress (10,11). An additional study shows that TIM is required for protecting stalled forks from uncontrolled nucleolytic degradation (12). Together, the FPC plays multifaceted roles in preserving the integrity of both active and stalled replication forks. While interactions between the FPC and multiple replication fork-associated factors, together with their posttranslational modifications, are expected to collectively govern the process of DNA replication, how the structure and function of the FPC is linked to coordinate diverse genome maintenance mechanisms remains largely uncharacterized.

The establishment of a bidirectional replication fork from an active origin leads to the DNA synthesis of leading and lagging strands due to the unidirectional nature of nucleotide incorporation to the 3′ ends of both daughter strands. Unlike Pol ε-dependent leading strand synthesis that occurs in a processive and continuous manner, discontinuous replication at lagging strands synthesizes a series of short DNA fragments named Okazaki fragments (OF) (13). OF synthesis is initiated with an RNA–DNA primer produced by Pol α-primase, which is extended by Pol δ until it encounters a downstream OF. Displacement of the 5′ end of the OF generates a single-stranded RNA flap, which is subsequently processed by the concerted action of flap endonuclease 1 (FEN1) and DNA2 nuclease, followed by DNA nick sealing via DNA ligase 1 (LIG1) to complete OF processing (14). If not properly controlled, the lagging strand maturation process becomes a source of genome instability as synthesis of short DNA fragments by Pol α is intrinsically prone to a high incidence of errors, and dysregulated processing of flap structures may cause DNA breakage and aberrant DNA structure formation. Accordingly, failure to seal the sheer number of OF, estimated to be over 10 million per cell cycle in humans, would create persistent single-strand breaks (SSBs) and gaps near replication forks, thereby leading to fork stalling and collapse (15).

Emerging evidence indicates that one failsafe mechanism of OF processing involves poly(ADP-ribosyl)ation, or PARylation, catalyzed mainly by poly(ADP-ribose) polymerase 1 (PARP1). PARP1 recognizes and is activated by DNA lesions, primarily DNA SSBs and double strand breaks (DSBs), which triggers the PARylation of PARP1 itself and other proteins involved in DNA damage repair (16). PARylation is transient by nature, which is short-lived with a half-life of less than 40 seconds, due to PAR glycohydrolase (PARG) activity (17). Importantly, steady levels of PARylation in the S phase of unperturbed cells are detected when PARG is inhibited, which is greatly increased when FEN1 or LIG1 is deficient, indicating that PARP proteins operate as a backup to fill unligated OF intermediates that may have escaped the canonical processing mechanism (18). PARP1-dependent recruitment of the scaffold protein XRCC1 and its partner DNA ligase III (LIG3) has been associated with this alternative OF maturation process for SSB and gap repair (19–21). Consequently, PARP inhibition impedes the maturation of nascent strands behind replication forks (22); this indicates that accumulation of OF intermediates is likely to be a major source of cytotoxicity associated with PARP trapping to DNA, which leads to excessive accumulation of ssDNA gaps and breaks under BRCAness, a feature of homologous recombination (HR) deficiency phenocopying germline mutations in *BRCA1* or *BRCA2*. How the PARP1-dependent DNA replication process coordinates with the lagging strand elongation catalyzed by the replisome is unknown.

In this study, using an auxin-inducible degron to acutely degrade TIM during S phase and an FKBP12-derived destabilization domain to disrupt the TIM–PARP1 complex, we identify that the TIM–PARP1 interaction at DNA replication forks is essential for the backup processing of OF intermediates to suppress replication-associated ssDNA gaps. We show that TIM is necessary for engaging PARP1 and its PARylation activity to recruit XRCC1 and facilitate the processing of unligated nascent DNA strands. Our study establishes a new connection between TIM and PARP1, two essential genome caretakers known to work at the intersection of DNA replication and repair, providing a new perspective on the FPC function to coordinate OF processing with replisome progression. We propose that combining the disruption of the TIM–PARP1 interaction with the suppression of canonical OF processing via FEN1 inhibition may be a therapeutic strategy valuable for cancer therapy by exacerbating replication-associated ssDNA gaps.

Materials and methods

Plasmid construction

pcDNA5/FRT/TO-Flag-TIM was constructed by subcloning Flag-TIM cDNA resistant to siRNA TIM-1 to pcDNA5/FRT/TO using KpnI and NotI restriction sites. EQ/EQ/TD mutations was introduced to full-length Flag-TIM cDNA by site-directed mutagenesis (SDM). pRetroX-pTuner DD TIM PAB-myc WT and EQ/EQ/TD were constructed by subcloning C-terminal myc-tagged TIM PAB (a.a. 882–1132) WT and EQ/EQ/TD (both synthesized by Genscript) into the pRetroX-pTuner DD backbone derived from Addgene plasmid #122082 using XhoI and NcoI restriction sites. All sequences were verified by Sanger DNA sequencing (Stony Brook Genomics Core Facility). PCR primer information can be found in Supplementary Table S1.

Cell culture and cell lines

U2OS and HEK293T cell lines were acquired from the American Tissue Culture Collection (ATCC). The HCT116 OsTRI1 F74G TIM-mAID cell line was previously described (23). Cells were cultured in Dulbecco's Modified Eagle's Medium (U2OS and HEK293T) or McCoy's 5A medium (HCT116 OsTIR1 F74G TIM-mAID) supplemented with 10% fetal bovine serum and 1% penicillin/streptomycin, following standard culture conditions and procedures. U2OS Flp-In T-REx TIM WT and EQ/EQ/TD cell lines were generated by co-transfecting pcDNA5/FRT/TO Flag-TIM and the pOG44 plasmid encoding the Flp recombinase (Invitrogen) into the host U2OS cell line stably expressing the Tet-repressor

(T-REx) and carrying a single FRT locus, followed by hygromycin selection and recovery of stably transfected cells after 4 weeks. Doxycycline was used at 100 ng/ml to drive cDNA expression following siRNA transfection. U2OS DD-PAB-myc TIM WT and EQ/EQ/TD cell lines were established by retroviral transduction of pRetroX-pTuner DD TIM PAB-myc, followed by 2 μg/ml puromycin selection.

DNA and siRNA transfection

Plasmid transfection was performed using GeneJuice (Millipore Sigma) according to the manufacturer's protocol. Transfection for the pRetroX-pTuner DD retrovirus production was performed using X-tremeGENE^{TM} HP DNA transfection reagent (Millipore Sigma). siRNA duplexes were transfected at 20 nM using Lipofectamine RNAiMAX (Thermo Fisher).

Drug treatments

5-Phenyl-1H-indole-3-acetic acid (5-Ph-IAA) was dissolved in DMSO to 10 mM stock and treated at 1 μM. LNT1 (FENi) was dissolved in DMSO to 10 mM stock and treated at 10, 5, or 1 μM. PDD 00017273 (PARGi) was dissolved in DMSO to 10 mM stock and treated at 10 μM. Shield-1 (Shld1) was dissolved in DMSO to 1 mM stock and treated at 1 μM.

Cell lysis and western blotting

Cells were trypsinized, washed once in ice-cold phosphate-buffered saline (PBS) and lysed in NETN300 (50 mM Tris–HCl [pH 7.5], 300 mM NaCl, 0.2 mM EDTA, 1% NP40) lysis buffer complemented with EDTA-free protease inhibitor cocktail (Millipore Sigma) and phosphatase inhibitor (Thermo Fisher) for 40 min on ice. For visualization of PAR signals, cells were lysed in modified RIPA buffer (50 mM Tris–HCl [pH 7.5], 150 mM NaCl, 1 mM EDTA, 1% NP-40, 0.5% SDS and 0.5% sodium deoxycholate) complemented with EDTA-free protease inhibitor cocktails and 10 μM PARGi. Following lysis, lysates were then clarified by centrifugation at 14,000 rpm at 4 °C for 10 min. Supernatant was collected and transferred into a microcentrifuge tube, and protein concentration was determined by Bradford assay. Thirty to 50 μg of protein was mixed with 2x sodium-dodecyl sulfate (SDS) containing 5% β-mercaptoethanol and boiled at 95 °C for 5 min. Samples were then subjected to SDS-polyacrylamide gel electrophoresis (PAGE) and transferred onto PVDF membrane. Membranes were blocked in 5% milk/bovine serum albumin (BSA) and then incubated with primary antibodies in tris-buffered saline (TBS) containing 0.1% Tween 20 (TBS-T) at 4 °C overnight. Following three washes in cold TBS-T, membranes were incubated with horseradish peroxidase (HRP)-conjugated secondary antibodies. The HRP signals were detected by enhanced chemiluminescence (ECL) western blotting substrates (Thermo Fisher) using the iBright Imaging System (CL1000; Thermo Fisher).

DNA fiber analysis

Exponentially growing cells were labeled with 50 μM 5-chloro-2′-deoxyuridine (CldU) for 30 min, washed three times with PBS and then labeled with 250 μM 5-iodo-2′-deoxyuridine (IdU) for 30 min prior to harvesting. Media was pre-equilibrated overnight at 37 °C in 5% CO_2. Cells were then permeabilized with CSK-100 buffer (100 mM NaCl, 10 mM MOPS [pH 7.0], 3 mM $MgCl_2$, 300 mM sucrose, 0.5% Triton X-100) for 10 min at room temperature (RT) and then washed once with PBS. Nuclei were then equilibrated with S1 endonuclease buffer (30 mM sodium acetate, 10 mM zinc acetate, 5% glycerol, 50 mM NaCl; final pH 4.6) for 5 min at RT and then treated with S1 endonuclease (20 U/ml) at 37 °C for 30 min. S1 endonuclease buffer was aspirated and, nuclei were precipitated with 0.1% BSA in PBS and collected using a cell scraper. The nuclei suspension was centrifuged at 7,000 rpm for 5 min at 4°C, and the supernatant was aspirated. The pellet was then resuspended in PBS such that ∼3000 nuclei could be lysed per sample. Two μl of the solution was dropped onto a positively charged glass slide, and fiber lysis solution (200 mM Tris–HCl [pH7.5], 50 mM EDTA, 0.5% SDS) was added on top of the drop followed by gently stirring with the pipette tip and incubation for 5–8 min. Slides were then carefully tilted by 15° to allow DNA fibers to spread along the slide and carefully placed horizontally to air dry for 10–15 min in the dark. DNA was fixed by immersing the slides in freshly prepared methanol/acetic acid solution (3:1) for 5 min at RT. Slides were allowed to dry and then washed twice in PBS for 5 min at RT. DNA was denatured in a 2.5 mM HCl solution for one hour at RT. Slides were washed three times in PBS for 5 min and placed horizontally. Slides were blocked with 5% BSA in PBS for 30 min, followed by incubation with rat monoclonal anti-BrdU (1:200) for CldU and mouse monoclonal anti-BrdU (1:20) for IdU, diluted in 1% BSA in PBS containing 0.025% Tween 20 (PBS-T) and incubated for 1.5–2 h at room temperature in a dark humidified chamber. Following three washes in PBS-T for 5 min each, two secondary antibodies (Alexa Fluor 594 goat anti-rat and Alexa Fluor 488 goat anti-mouse, 1:400 each) were diluted in 1% BSA in PBS and incubated for one hour at RT in a dark humidified chamber. Slides were washed three times in PBS-T for 5 min each and allowed to dry completely in the dark. Coverslips were placed on top of the slides coated with ProLong^{TM} Gold Antifade Mountant (Thermo Fisher) and allowed to cure overnight at RT. DNA fibers were imaged with an Eclipse Ts2R-FL inverted fluorescence microscope (Nikon) equipped with a Nikon DSQi2 digital camera and analyzed using NIS-Elements, Research BR software (Nikon).

Immunofluorescence

Cells were transfected and/or treated with the specified drugs and then seeded onto a glass coverslip. TIM-mAID cells were seeded onto coverslips pre-coated with poly-L-lysine. Cells were pulse-labelled with 10 μM EdU for 30 min prior to fixation with 4% paraformaldehyde at RT for 10 min and then permeabilized with 0.3% Triton X-100 in PBS on ice for 3 min. For visualizing XRCC1 foci, cells were pre-extracted with 0.5% Triton X-100 in PBS on ice for 5 min before fixation. Coverslips were blocked with 5% BSA in PBS-T at RT for 1h. Coverslips were then incubated with primary antibodies diluted in 1% BSA in PBS-T for 1.5–2 h at 37 °C. Coverslips were then briefly washed with PBS-T and then incubated with the indicated secondary antibodies for 1 h at RT. For EdU-labelled cells, click reaction was performed with Alexa Fluor 647 azide using the Click-iT reaction cocktail according to the manufacturer's protocol (Thermo Fisher) for 30 min at RT. Coverslips were mounted in VECTASHIELD mounting media with DAPI and sealed with clear nail polish. At least 250 nuclei were analyzed for each condition with an Eclipse Ts2R-FL inverted fluorescence microscope.

Proximity ligation assay (PLA)

Exponentially growing cells were seeded onto coverslips and treated with the specified drugs. Coverslips were washed once with PBS and then fixed with 4% paraformaldehyde at RT for 10 min followed by permeabilization with 0.3% Triton X-100 in PBS on ice for 3 min. Coverslips were blocked with blocking buffer (Duolink *In situ* PLA Probe kit) for 1 h at 37 °C. Coverslips were then incubated with primary antibodies diluted to the desired concentrations in antibody diluent (Duolink *In situ* PLA Probe kit) for 1 h at 37 °C. Coverslips were then washed three times with RT wash buffer A for 5 min each and then incubated with 1x PLA MINUS and PLUS probes diluted in antibody diluent (Duolink *In situ* PLA Probe kit) for 1 h at 37°C. Coverslips were washed three times with wash buffer A for 5 min each and incubated with ligase diluted 1:80 in 1× ligation buffer (Duolink *In situ* Detection Reagents) for 30 min at 37 °C. Coverslips were then washed and incubated with polymerase diluted 1:40 in 1× amplification buffer (Duolink *In situ* Detection Reagents) for 1 h 40 min at 37 °C. Coverslips were then washed three times with RT wash buffer B for 10 min each. All the reactions were performed in in a humidified chamber. Coverslips were then mounted in mounting media containing DAPI. To visualize the proximity to EdU-labeled replication forks, cells were pulse-labeled with 125 μM EdU and pulsed with 1 mM thymidine before harvest. After washing and blocking, biotin azide was conjugated to EdU via click reaction using the Click-iT reaction cocktail according to the manufacturer's protocol (Thermo Fisher), followed by antibody incubation. For multicolor PLA to detect the TIM–PARP1 interaction at EdU-labeled replication forks, fixed cells after click reaction were incubated with mouse anti-PARP1 (1:500) and goat anti-biotin (1:8000) primary antibodies diluted in antibody diluent (Duolink *In situ* PLA Probe kit) for 1 h at 37 °C for green PLA. For far red PLA, rabbit anti-TIM and goat anti-biotin antibodies were first conjugated to oligo H and oligo I respectively using Duolink PLA Multicolor Probemaker Kit, Far Red, according to the manufacturer's protocol, followed by incubation of TIM-oligo H and biotin-oligo I conjugated PLA probes diluted to the desired concentrations in 1x probe diluent. Amplification of specific PLA probe pairs was performed using Duolink *In Situ* Detection Reagents, Green for the PARP1-EdU PLA and Duolink PLA Multicolor Reagent Pack for the TIM-EdU PLA (far red). An additional detection step was carried out by incubating the coverslips in Duolink PLA Multicolor detection buffer diluted in high purity water for 30 min at 37 °C. All wash steps were performed for twice the length of time as previously discussed to eliminate extensive background signal. Proximity of two overlapping PLA foci results in white PLA signals.

Cell synchronization

Cells were synchronized at the G1/S boundary using double thymidine block. Thymidine was dissolved in PBS at 100 mM stock and treated at 2 mM. Cells were seeded at 30% confluency, allowed to attach for 24 h and then treated with 2 mM of thymidine in cell culture media for 17 h. Cells were washed three times with warm PBS and replenished with fresh thymidine-free media for 9 h. Cells were subsequently treated with a second dose of 2 mM thymidine for 17 h before being released into fresh media as indicated. For all steps, media was pre-equilibrated overnight at 37 °C in 5% CO_2.

Flow cytometry

Cell cycle analysis was performed by flow cytometry on exponentially growing cells treated with the drugs as specified. To measure EdU incorporation, exponentially growing cells were treated with 10 μM EdU for 30 min and washed once before harvest. After one PBS wash, cells were washed with 1% BSA in PBS, vortexed briefly and centrifuged at 500 g for 5 min at RT. Cells were resuspended into a single-cell solution in PBS and fixed with 70% ethanol for 2 h on ice in the dark. Ethanol was removed by centrifugation at 500 g for 5 min and one PBS wash. Cells were subjected to EdU-click reaction using Alexa Fluor 488 picolyl azide and click-iT plus EdU flow cytometry assay kit (Thermo Fisher) following the manufacturer's protocol. To detect γH2AX levels, harvested cells were permeabilized using 0.5% Triton X-100 at 4 °C for 10 min. Cells were washed with 1% BSA in PBS and fixed in Foxp3/transcription factor fixation solution (Thermo Fisher) for 1 h at RT. Cells were then washed with Foxp3/transcription factor permeabilization buffer, centrifuged at 400 g for 5 min, and incubated with Alexa Fluor 488-conjugated γH2AX (1:100; CR55T33, Thermo Fisher) for 1 h at RT in the dark. Cells were washed once with PBS and resuspended in PBS containing 200 μg/ml PureLink™ RNase and eBioscience ™ 7-AAD viability staining solution (Thermo Fisher) and incubated at 37 °C for 30 min. Samples were analyzed with the Attune NxT acoustic focusing cytometry (Thermo Fisher) and the Attune NxT software v2.7 (Thermo Fisher).

Cell survival and colony formation assays

To measure cell viability, cells were seeded in 96-well plates and allowed to attach for 24 h. Drugs were treated as specified, and cell viability was determined using the CellTiter-Glo luminescent cell viability assay (Promega) four days later. ATP-derived luminescence was measured by the GloMax Explorer microplate reader (Promega). To assess colony formation, cells were seeded in 6-well plates and treated with the specified drugs for the indicated times. On day 12, cells were washed once with cold PBS and fixed with ice-cold methanol for 10 min at −20 °C. Cells were then washed with PBS and incubated in 0.5% crystal violet solution for 10 min at RT in the dark. Crystal violet was solution was removed, and the excess stain was washed off gently with deionized water. Once dried, colonies were counted manually.

Isolation of proteins on nascent DNA (iPOND)

One hundred million of exponentially growing TIM-mAID cells were treated with the drugs as specified. Cells were incubated with 10 μM PARGi for 20 min and pulse-labeled with 10 μM EdU during the last 12 min. Following one wash with PBS, DNA-protein complexes were crosslinked with 1% formaldehyde for 20 min and quenched with 0.125 M glycine. Following harvest, cells were permeabilized with 0.25% Triton X-100 in PBS for 30 min at RT and washed three times with PBS. To conjugate EdU with biotin azide, click reaction was carried out following the manufacturer's protocol (Thermo Fisher) for 2 h at RT. Cells were washed three times with PBS and resuspended with modified lysis buffer (50 mM Tris-HCl [pH 8.0] and 1% SDS) supplemented with protease inhibitors and 10 μM PARGi. DNA was fragmented by sonication using a microtip sonicator 550 Sonic Dismembrator (Thermo Fisher) for 3 min (30 s on, 60 s off ×2) at 4°C

followed by centrifugation at 13 000 rpm for 10 min. 0.1% of the supernatant was collected as input and the remaining sample was diluted 1:1 with PBS supplemented with protease inhibitors and 10 μM PARGi and incubated overnight with streptavidin agarose beads at 4°C. Beads were washed twice with low salt buffer (1% Triton, 20 mM Tris–HCl [pH 8.0], 2 mM EDTA, 150 mM NaCl), twice with high salt buffer (1% Triton, 20 mM Tris–HCl [pH 8.0], 2 mM EDTA, 500 mM NaCl), and twice with lysis buffer. Proteins were eluted by boiling beads in 2× Laemmli buffer for 30 min at 95°C. The samples were centrifuged at 14,000 pm for 15 min and the supernatants were loaded onto SDS-PAGE gels for western blot analysis.

Statistics and reproducibility

All statistical analyses were performed using Prism (GraphPad), where n.s., $P > 0.05$; *, $P < 0.05$; **, $P < 0.01$; ***, $P < 0.001$; ****, $P < 0.0001$. All of the statistical details of experiments can be found in the figures and figure legends. Unpaired Student's t-tests were performed with a 95% confidence interval, using two-tailed *P*-values, unless otherwise specified. For DNA fiber assays, DNA track lengths were measured by Fiji, and a two-side Mann–Whitney *U* test was conducted with a 95% confidence interval on a set of DNA fiber samples over 150. Dot plots depict a representative result of at least two independent biological replicates and analysis by Mann–Whitney *U* test. Western blotting, cell survival assay, clonogenic assay, immunofluorescence, PLA and flow cytometry experiments were representative of at least two, mostly three, biologically independent experiments, to demonstrate reproducibility.

Results

siRNA-mediated TIM depletion leads to accumulation of ssDNA gaps and increased PARylation

In order to determine the impact of TIM loss in replication-associated ssDNA gap accumulation, we first knocked down TIM and incorporated the ssDNA-specific S1 nuclease into a DNA fiber assay (24), which cleaves the gap generating a shorter IdU track in the CldU/IdU-labeled DNA in comparison to S1 non-treated control (Figure 1A). Knocking down TIM using two independent siRNAs (Figure 1B) led to shortening of DNA replication tracks as previously noted (12), which decreased significantly upon treatment of S1 nuclease, indicating that ssDNA gaps are accumulating while fork progression is being impaired in the absence of TIM (Figure 1C).

The phenotype of TIM loss in ssDNA gap accumulation is shared by the loss of PARP1 or PARP1 inhibition, which leads to an increase in post-replicative single-strand nicks or gaps caused by the accumulation of unligated OF during replication fork progression (18,22). Of note, previous structural and biochemical studies demonstrated that the C-terminus of TIM directly interacts with PARP1 (25,26). We therefore reasoned that the TIM–PARP1 interaction at DNA replication forks may play an important role in replication fork progression, especially for lagging strand synthesis by controlling the processing of OFs. Using a multicolor proximity ligation assay (PLA) that we modified from *in situ* protein interactions at nascent and stalled replication forks (SIRF), we confirmed that TIM and PARP1 colocalize at ongoing replication forks labeled with a thymidine analog, EdU (Supplementary Figure S1A). A series of electrostatic interactions that are required for the TIM–PARP1 interaction were revealed by X-ray crystallography (25); based on this information, we previously established a TIM mutant (E1049Q/E1056Q/T1078D; hereinafter EQ/EQ/TD) that is unable to interact with PARP1 (Supplementary Figure S1B) (27). A co-immunoprecipitation assay confirmed that the Flag-tagged TIM EQ/EQ/TD mutant fails to interact with endogenous PARP1 (Supplementary Figure S1C). This mutant maintains its interaction with other interacting partners TIPIN or SDE2, indicating the overall replisome integrity is not compromised (12,27). Using the Flp-In T-REx system, siRNA-resistant wild-type (WT) or the EQ/EQ/TD mutant was reconstituted into TIM knocked-down cells in a doxycycline-dependent manner (Supplementary Figure S1D). Our initial analyses demonstrated that cells expressing the EQ/EQ/TD mutant exhibit impaired replication fork progression and stalled fork protection (27). Here, we further showed that while re-expression of WT TIM in TIM-depleted Flp-In cells suppressed the ssDNA gaps, thus confirming specificity of the phenotype observed in TIM knockdown (Supplementary Figure S1E), cells expressing the TIM EQ/EQ/TD mutant failed to counteract the effect of S1 treatment, suggesting that the TIM–PARP1 interaction is required for suppressing ssDNA gap accumulation (Figure 1D). Notably, ssDNA gap formation was still evident in *PRIMPOL*-knockout cells, indicating that repriming only partially accounts for the ssDNA gaps manifested by the absence of TIM (Supplementary Figure S1F).

Since the catalytic activity of PARP1 at DNA replication forks is associated with preventing ssDNA gaps by supporting lagging strand synthesis, we evaluated how cellular PARylation is affected without TIM. Notably, depletion of TIM resulted in a drastic increase in PAR signals as revealed by anti-PAR immunofluorescence, which was more readily observed when PARG activity was inhibited as a means to capture transient PARylation engaged for OF processing during DNA replication (Figures 1E, F). Analysis of cellular PARylation by anti-PAR immunoblotting exhibited a similar increase when TIM was knocked down (Figure 1G). In S phase cells marked by EdU, the EQ/EQ/TD mutant was not able to fully suppress the elevated PAR levels resulting from TIM depletion, underscoring the importance of the TIM–PARP1 interaction in the process (Supplementary Figure S1G). However, the increase of PARylation was noted in both EdU-positive and negative cell populations, suggesting that elevated PAR signals are not necessarily DNA replication-dependent; rather, it may represent the non-specific cytotoxicity caused by long-term TIM knockdown and impairment of overall DNA replication fork integrity (Figure 1F). Indeed, cells depleted of TIM by siRNA exhibited elevated pKAP1 S824 and γH2AX signals, which represent DNA damage and breaks, and accumulation of cleaved PARP1 (cPARP1), which is a sign of apoptosis (Figures 1H, S1H). Together, while TIM deficiency greatly elevates the level of ssDNA gaps, it is accompanied by a significant increase in cellular PARylation. Therefore, its effect may not be directly related to DNA damage stemming from normal DNA replication processes; instead, excessive PARylation may represent global DNA breakage and genomic damage.

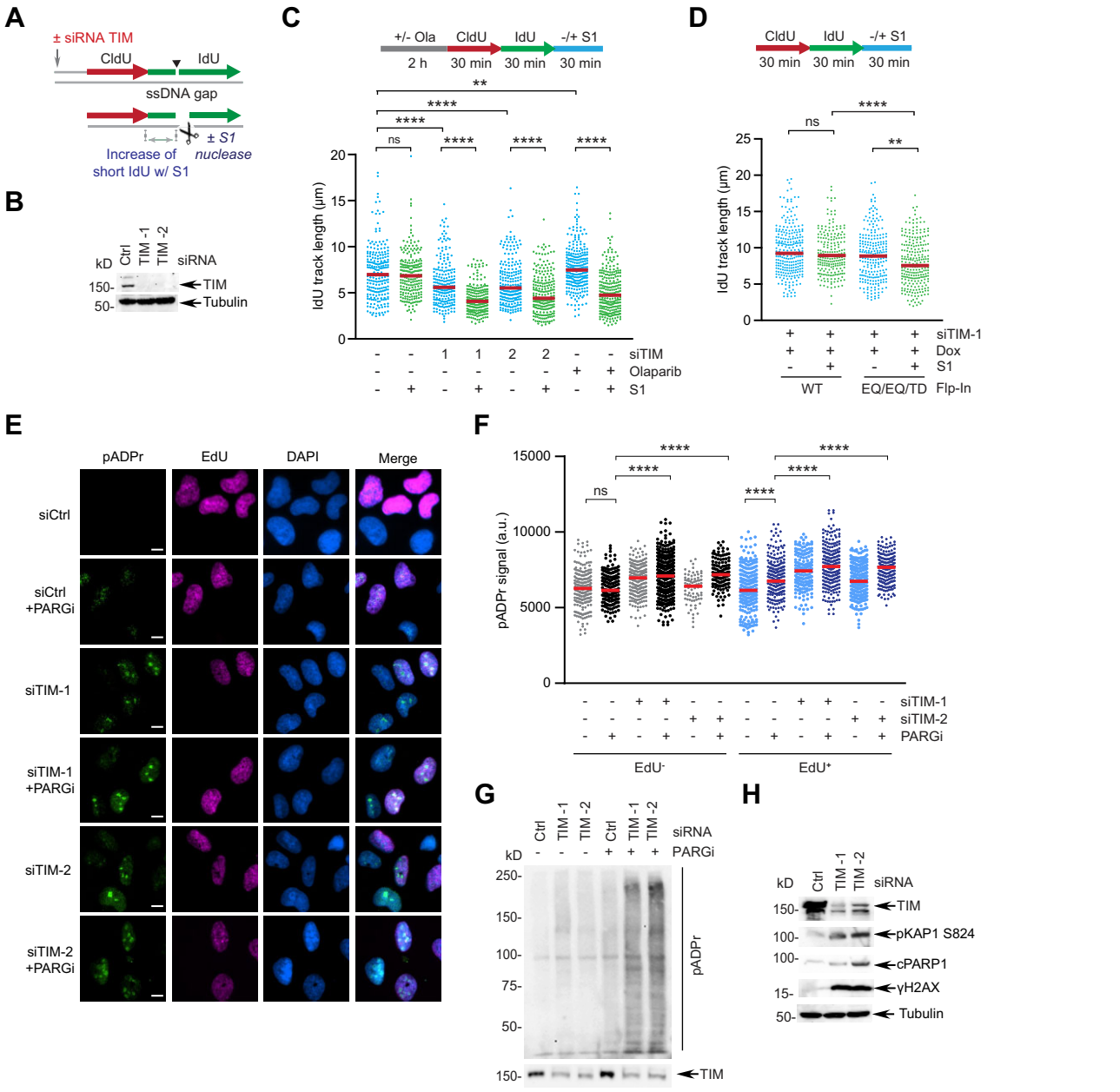

Figure 1. siRNA-mediated TIM knockdown results in increased DNA damage and ssDNA gap accumulation. (**A**) Schematic of the DNA fiber assay with S1 endonuclease. (**B**) Western blotting (WB) confirming the knockdown of TIM in U2OS cells using two independent siRNA oligonucleotides (versus negative control, Ctrl). (**C**) Dot plot of the DNA fiber IdU track lengths from U2OS cells depleted of TIM by siRNA. Where indicated, 20 U/ml S1 nuclease was treated for 30 min. 10 µM olaparib was treated for 2 h as a positive control to induce DNA gaps. Red bars indicate the median value of at least 150 tracks. $n = 3$, $^{****}P < 0.0001$, $^{**}P < 0.01$, Mann–Whitney. (**D**) Dot plot of the DNA fiber IdU track lengths from Flp-In cells reconstituted with Flag-tagged TIM WT or EQ/EQ/TD via siRNA-mediated TIM knockdown and doxycycline (dox)-dependent expression of siRNA-resistant cDNA. Where indicated, cells were treated with 20 U/ml S1 nuclease for 30 min. Red bar: median, $n = 3$, $^{****}P < 0.0001$, $^{**}P < 0.001$, ns: not significant, Mann–Whitney. (**E**) Representative images of poly(ADP-ribose) or pADPr signals in U2OS cells knocked down of TIM using two independent siRNA. Where indicated, cells were treated with 10 µM PARGi for 30 min before fixation. Scale bar: 10 µm. (**F**) Quantification of pADPr immunofluorescence signals in either EdU negative or EdU positive cells. At least 250 cells were analyzed in each condition. Red bar: median, $n = 3$, $^{****}P < 0.0001$, ns: not significant, Mann–Whitney. (**G**) WB analysis of cellular pADPr levels in U2OS cells transfected with siRNA TIM (versus Ctrl) in the presence or absence of 10 µM PARG inhibitor (PARGi). (**H**) WB analysis of DNA damage in U2OS cells transfected with siRNA TIM (versus Ctrl) for 72 h.

Acute TIM degradation causes ssDNA gap accumulation accompanied by a decrease in PARP1 activity

To overcome the limitation of long-term TIM knockdown, which causes DNA breaks and thus genome-wide PARP activation, we turned to implement the TIM auxin-inducible degron (AID) system that we previously established in HCT116 cells (a.k.a. HCT116-TIM mAID) (23) (Figure 2A). In this system, treatment with an auxin-derivative, 5-Ph-IAA, rapidly triggers TIM degradation from DNA replication forks within an hour, enabling us to specifically monitor the effect of acute TIM loss without non-specific toxicity of long-term TIM knockdown (Figure 2B). The cellular levels of TIPIN, the heterodimeric partner of TIM within the FPC, remained unchanged, indicating that the overall integrity of the replisome has not been compromised. Accordingly, after administration of 5-Ph-IAA for 6 h, pCHK1 activation, which requires TIPIN within the FPC, still occurred under hydroxyurea (HU)-induced replication stress (Supplementary Figure S2A). Induction of complete TIM degradation within 3 h did not cause any major DNA replication damage signals in contrast to 48 h, a time point that essentially mimicked the phenotypes manifested in siRNA-mediated TIM knockdown (Supplementary Figure S2B). Incorporation of EdU was largely unaffected upon administration of 5-Ph-IAA for 3 h, indicating that DNA replication forks have not yet experienced considerable stalling yet (Supplementary Figure S2C). In this condition, DNA fiber tracks obtained from cells treated with 5-Ph-IAA were comparable to the untreated, while S1 treatment in the DNA fibers revealed that ssDNA gaps rapidly accumulated within 3 h upon acute loss of TIM (Figure 2C). The S1-sensitive ssDNA gaps were further evident in later time points when the progression of DNA replication forks starts to become compromised (Supplementary Figure S2D). Therefore, we conclude that acute TIM degradation at ongoing forks results in ssDNA gap accumulation without a major impact on fork progression.

Interestingly, acute TIM degradation led to a progressive decrease of PARylation that was detectable by PARG inhibition under immunofluorescence at 2 and 4 h post 5-Ph-IAA, whereas prolonged 5-Ph-IAA treatment for 24 and 48 h resulted in a massive increase in PARylation even in EdU-negative cells (Figures 2D, E). Long-term depletion of TIM in parental HCT116 cells by siRNA also resulted in ssDNA gap accumulation and a dramatic increase of cellular PARylation as noted in siRNA-treated U2OS cells (Supplementary Figure S2E and S2F). Our TIM degron model therefore suggests that TIM is required for steady-level PARylation at sites of DNA synthesis and further supports the previous notion that long-term loss of TIM leads to non-specific PARP activation. To further substantiate our results, we synchronized HCT116-TIM mAID cells at the G1/S boundary and released cells into S phase in the presence or absence of 5-Ph-IAA to monitor S phase-specific PARylation. Again, rapid TIM degradation suppressed the PAR levels that were progressively increased during DNA replication in control cells when captured by PARG inhibition (Figure 2F). We were also able to observe a decrease in PARylation at ongoing replication forks by immunoblotting upon acute TIM degradation (Figure 2G). Together, our TIM degron system identified a unique role of TIM in promoting PARylation and suppressing ssDNA gaps at ongoing DNA replication forks.

TIM promotes PARP1-dependent backup Okazaki fragment processing

Previous studies established the role of PARP1 in lagging strand synthesis by filling unligated OF intermediates that escape the canonical OF maturation process mediated by FEN1 and LIG1 (18,22,28). Therefore, we examined whether positive regulation of PARylation by TIM during DNA replication is linked to the backup OF processing promoted by the PARP1 activity at DNA replication forks. Consistent with previous reports, we observed a dramatic elevation of PAR signals when the canonical OF processing is inhibited by either LIG1 knockdown or FEN1 inhibition, and this increase was suppressed when TIM was rapidly depleted by 5-Ph-IAA, indicating that TIM is required for the PARP activity necessary for engaging the backup OF processing pathway (Figure 3A). A massive accumulation of PARylation upon LIG1 knockdown was also visualized by immunoblotting, which was suppressed by 5-Ph-IAA (Figure 3B). Accordingly, ssDNA gaps were further accumulated when FEN1 was inhibited and TIM was degraded by 5-Ph-IAA simultaneously (Figure 3C). In contrast, the elevated PARylation caused by genome-wide SSB accumulation upon methyl methanesulfonate (MMS) was not suppressed by TIM degradation, indicating that the role of TIM to support PARylation is specific to DNA replication (Supplementary Figure S3A). Furthermore, FEN1i-induced PARylation was moderately decreased by Pol α inhibition, supporting that PARP activation originates from defective lagging strand synthesis (Supplementary Figure S3B). Modification of PARP1 or other nearby proteins with PAR leads to the recruitment of the XRCC1 SSB repair protein partnering with LIG3 to repair ssDNA gaps as well as flaps or nicks (29,30). We used a pre-extraction protocol to visualize XRCC1 foci that became obvious upon FEN1 inhibition in HCT116 TIM-mAID cells (Supplementary Figure S3C). Similarly, LIG1 knockdown increased the XRCC1 foci formation, and 5-Ph-IAA treatment was sufficient to abrogate the XRCC1 foci, indicating that the PARP1-dependent backup SSB repair pathway is defective in the absence of TIM (Figures 3D, E). Collectively, our results indicate that TIM is required for the PARP1 activity toward unligated OF processing to support lagging strand synthesis.

The TIM–PARP1 interaction is required for PARP1-dependent OF processing and ssDNA suppression

To further understand the mechanism through which TIM promotes the PARP1 activity necessary for unligated OF processing at DNA replication forks, we determined whether the physical interaction between TIM an PARP1 is required for this process. Since our Flp-In system shown in Figure 1 may exhibit non-specific DNA damage that is generated during the process of siRNA-mediated TIM depletion and re-expression of cDNA encoding TIM WT or the PARP1-binding mutant, we wished to implement a system that allows us to acutely disrupt the endogenous TIM–PARP1 interaction without compromising the role of TIM in supporting the replisome. To this end, we employed inducible expression of a fragment derived from the C-terminus of TIM to compete with its binding to endogenous PARP1. Here, the TIM C-terminal PARP1-binding region (PAB) is fused to a myc tag and a FKBP12-derived destabilization domain (DD), referred to as DD-PAB-myc. Expression of DD-PAB-myc in cells enforces the PAB

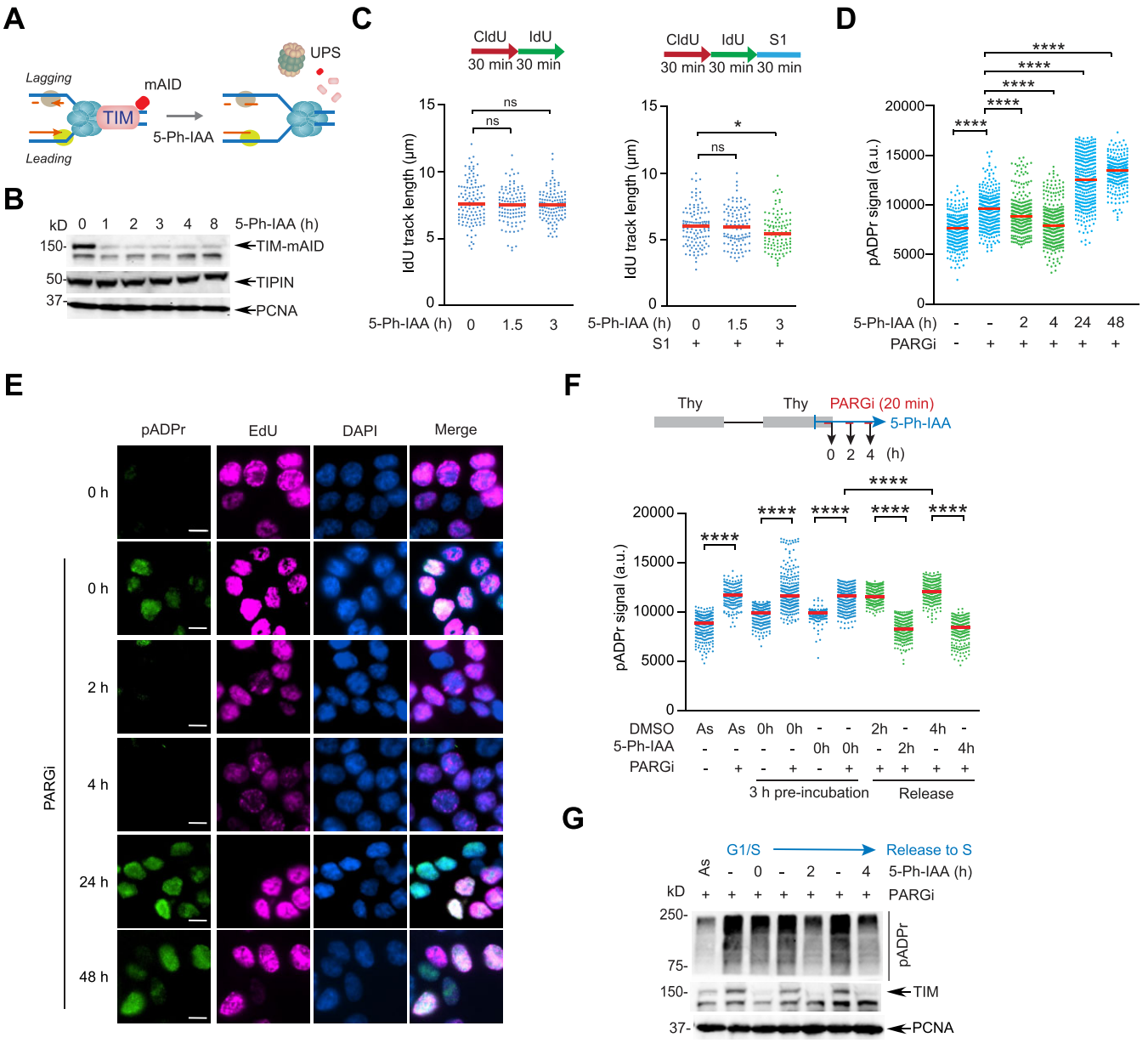

Figure 2. Acute TIM degradation results in a failure to activate S-phase specific PARylation. (**A**) Top: Schematic depicting auxin (5-Ph-IAA)-inducible acute degradation of endogenous TIM tagged with a mini-AID (mAID) degron by ubiquitin-dependent proteasome system (UPS) at an ongoing DNA replication fork. (**B**) WB to demonstrate rapid degradation of TIM-mAID in HCT116 cells upon treatment of 1 μM 5-Ph-IAA for the indicated times. Specific loss of TIM without depleting its heterodimeric partner TIPIN suggests that the overall replisome integrity is not compromised at early time points of TIM loss. (**C**) Dot plot of the DNA fiber IdU track lengths of TIM-mAID cells treated with 1 μM 5-Ph-IAA for the indicated times in the presence and absence of S1 endonuclease. Red bar: median, $n = 2$, $^{*}P < 0.05$, ns: not significant, Mann–Whitney. (**D**) Dot plot representing the quantification of total pADPr intensity in TIM-mAID cells following treatment with 1 μM 5-Ph-IAA (vs. DMSO) for the indicated times. Where indicated, 10 μM PARGi was treated for 20 min before fixation. Red bar: median, $n = 3$, $^{****}P < 0.0001$, Mann–Whitney. (**E**) Representative images of pADPr immunofluorescence staining. Scale bar: 10 μm. (**F**) Dot plot representing the quantification of total pADPr intensity in TIM-mAID cells in S phase. Cells were synchronized at the G1/S boundary by double thymidine block and incubated with either DMSO or 1 μM 5-Ph-IAA for 3 h before release into fresh media in the presence of DMSO or 5-Ph-IAA for 0, 2 and 4 h. Where indicated, cells were treated with 1 μM PARGi for 20 min before fixation. Red bar: median, $n = 2$, $^{****}P < 0.0001$, Mann–Whitney. (**G**) WB to visualize cellular pADPr levels in TIM-mAID cells synchronized at the G1/S boundary and released to S phase with or without 1 μM 5-Ph-IAA. Cells were treated with 10 μM PARGi for 20 min before harvest.

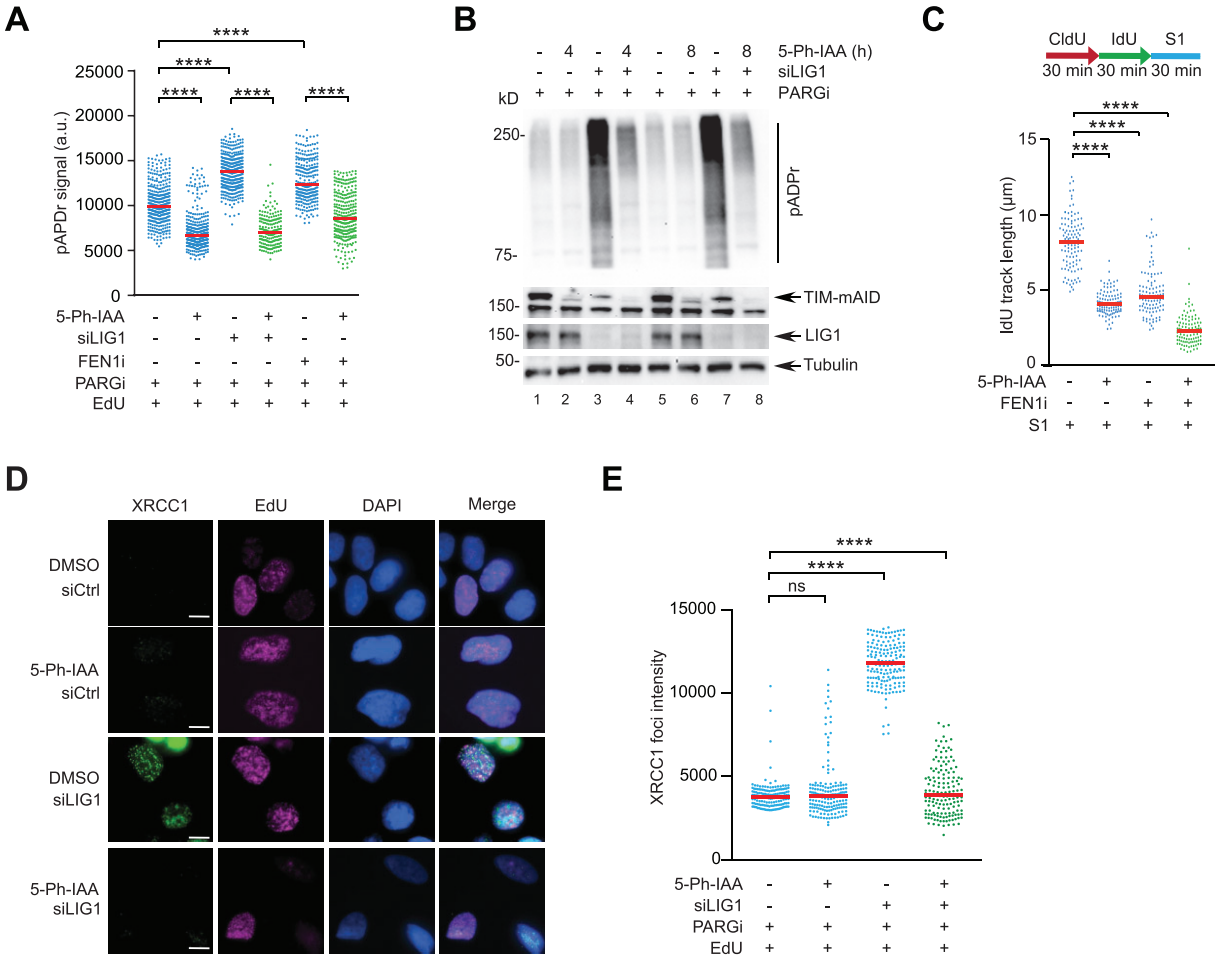

Figure 3. TIM is required for PARP1-dependent backup Okazaki fragment processing. (**A**) Dot plot representing the quantification of S phase-specific pADPr intensity from EdU-positive TIM-mAID cells treated with 1 μM 5-Ph-IAA for 4 h. Cells were either transfected with siRNA LIG1 (vs. Ctrl) for 66 h or treated with 1 μM FEN1 inhibitor (LNT1: FEN1i) for 4 h, and co-treated with 10 μM PARGi and 10 μM EdU for 30 min prior to fixation. Red bar: median, $n = 3$, $^{****}P < 0.0001$, Mann–Whitney. (**B**) WB to visualize cellular pADPr levels in TIM-AID cells transfected with siRNA LIG1 (versus Ctrl) for 66 h and/or treated with 1 μM 5-Ph-IAA for the indicated times. (**C**) Dot plot of the DNA fiber IdU track lengths from TIM-mAID cells treated with 1 μM 5-Ph-IAA for 8 h and/or 1 μM FEN1i for 1 h. S1 endonuclease was applied to assess ssDNA gap accumulation. Red bar: median, $n = 2$, $^{****}P < 0.0001$, Mann–Whitney. (**D**) Representative images of XRCC1 immunofluorescence staining in TIM-mAID cells transfected with siRNA LIG1 for 66 h and/or treated with 1 μM 5-Ph-IAA for 4 h. Cells were treated with 10 μM EdU for 30 min, and 10 μM PARGi was added during the last 20 min before pre-extraction with 0.5% Triton X-100 in PBS to detect chromatin-bound XRCC1. (**E**) Dot plot representing XRCC1 foci. Total XRCC1 intensity was quantified from EdU-positive cells to determine the XRCC1 foci intensity. Red bar: median, $n = 2$, $^{****}P < 0.0001$, ns: not significant, Mann–Whitney.

to undergo rapid proteasomal degradation unless its stability is preserved by the addition of Shield-1 (Shld1), a FKBP ligand (31); stabilized TIM PAB would compete with endogenous TIM for the binding interface of PARP1, thereby rapidly disrupting the TIM–PARP1 interaction (Figure 4A). We also introduced EQ/EQ/TD mutations into DD-PAB-myc to use as a control polypeptide that cannot disrupt the TIM–PARP1 interaction. Stable expression of both DD-PAB-myc WT and EQ/EQ/TD mutant in U2OS cells revealed that both fragments are barely expressed due to rapid proteolysis, while they are readily induced at comparable levels upon treatment with Shld1 (Figure 4B). The induction of DD-PAB-myc WT was dose-dependent and time-dependent, which was detectable as early as 2 h post Shld1 and plateaued around 24 h (Supplementary Figures S4A, S4B). The inducible expression of DD-PAB-myc by Shld1 was comparable to the transient transfection of cDNA encoding full-length myc-tagged TIM, substantiating the robust induction of DD-PAB-myc in our system (Supplementary Figure S4C).

We next validated the DD-PAB-myc system as a means to disrupt the TIM–PARP1 interaction. The proximity ligation between TIM and PARP1 revealed that induction of DD-PAB-myc WT by Shld1 for 8 h results in a decrease in the PLA foci which is abrogated within 24 h; DD-PAB-myc EQ/EQ/TD mutant failed to do so, indicating that the TIM–PARP1 interaction is disrupted specifically by the PAB fragment (Figures 4C, D). Similarly, Shld1 decreased multicolor TIM and PARP1 PLA at EdU-labeled replication forks in cells expressing the WT, but not the EQ/EQ/TD mutant, PAB fragment (Supplementary Figure S4D). Importantly, expression of DD-PAB-myc WT, but not the EQ/EQ/TD mutant, was sufficient to induce ssDNA gap accumulation, suggesting that the TIM–PARP1 interaction is required for suppressing ssDNA gap formation (Figure 4E). Furthermore, the PARylation at DNA replication forks, as detected upon PARG inhibition, was specifically suppressed by DD-PAB-myc WT, but not by the mutant, indicating that the TIM–PARP1 interaction during DNA replication contributes to PARP1 activity

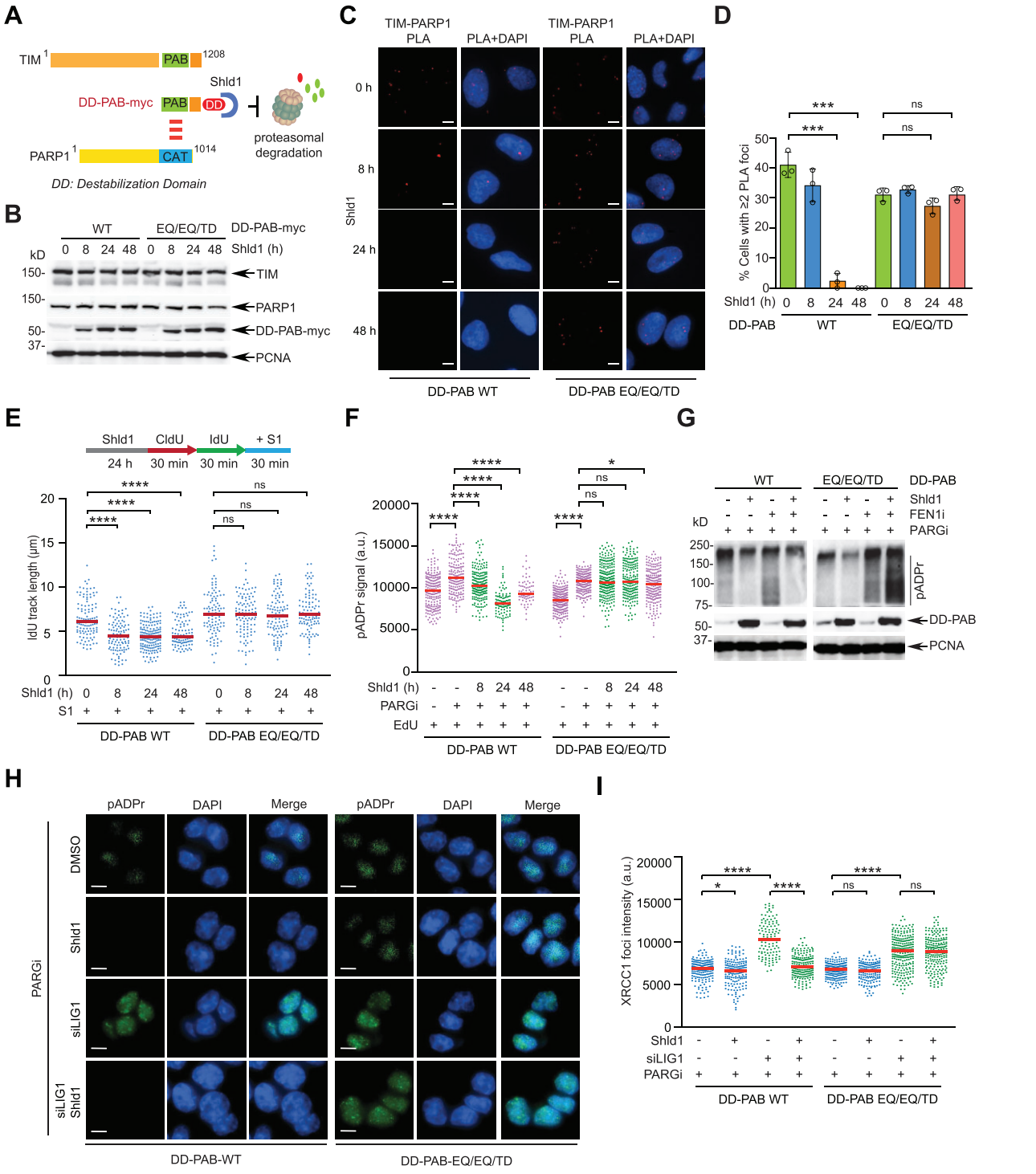

Figure 4. Physical disruption of the TIM–PARP1 interaction impairs PARP1-dependent OF processing. (**A**) Schematic depicting a strategy to disrupt the TIM–PARP1 interaction in an inducible manner. The C-terminal PARP1-binding region (PAB) of TIM fused to a destabilization domain (DD) is short-lived via rapid proteasomal degradation but stabilized by a synthetic ligand Shield-1 (Shld1), thus competing with endogenous TIM to disrupt its interaction with PARP1. (**B**) WB to show the induction of myc-tagged DD-PAB wildtype (WT) or EQ/EQ/TD mutant in cells treated with 1 μM Shld1 for the indicated times. (**C**) Representative images of the TIM–PARP1 PLA foci from U2OS DD-PAB WT or EQ/EQ/TD mutant cells following treatment of 1 μM Shld1 for the indicated times. Scale bar: 10 μm. (**D**) Quantification of cells positive for the TIM–PARP1 PLA foci. $n = 3$, mean ± SD, $^{***}P < 0.001$, ns: not significant, Student's *t*-test. (**E**) Dot plot of the DNA fiber IdU track lengths of DD-TIM-PAB WT or EQ/EQ/TD mutant cells following treatment of 1 μM Shld1 for the indicated times. Red bar: median, $n = 2$, $^{****}P < 0.0001$, ns: not significant, Mann–Whitney. (**F**) Dot plot representing the quantification of S phase-specific pADPr intensity from EdU-positive DD-TIM-PAB WT or EQ/EQ/TD mutant cells treated with 1 μM Shld1 for the indicated times. Red bar: median, $n = 2$, $^{****}P < 0.0001$, $^{*}P < 0.05$, ns: not significant, Mann–Whitney. (**G**) WB to visualize cellular pADPr levels in DD-TIM-PAB WT or EQ/EQ/TD mutant cells treated with 10 μM FEN1i for 4 h and/or 1 μM Shld1 for 8 h. 10 μM PARGi was treated for 20 min before harvest. (**H**) Representative images of pADPr signals in DD-TIM-PAB WT or EQ/EQ/TD mutant cells transfected with siRNA LIG1 for 66 h and/or treated with 1 μM Shld1 for 8 h. 10 μM PARGi was treated for 20 min before fixation. **(I)** Dot plot representing S phase-specific XRCC1 foci intensity in EdU-positive DD-TIM-PAB WT or EQ/EQ/TD mutant cells transfected with siRNA LIG1 for 66 h and/or treated with 1 μM Shld1 for 8 h. Red bar: median, $n = 2$, $^{****}P < 0.0001$, $^{*}P < 0.05$, ns: not significant, Mann–Whitney.

(Figures 4F, Supplementary Figure S4E). Disruption of the TIM–PARP1 interaction by DD-PAB WT, but not by the EQ/EQ/TD mutant, also rendered cells unable to elevate PARylation in response to FEN1 inhibition or LIG1 deficiency, as revealed by immunoblots and immunofluorescence, supporting the notion that the TIM–PARP1 interaction is necessary for engaging PARP1 to the backup pathway to repair unligated OF intermediates (Figures 4G, H; for quantification, see Supplementary Figure S5A). Consequently, cells in which DD-PAB-myc WT was induced exhibited shorter DNA tracks in comparison to cells with or without induction of the EQ/EQ/TD mutant, indicating that a defect in lagging strand synthesis is linked to impaired fork progression (Supplementary Figure S5B). Likewise, induction of DD-PAB-myc WT, but not the mutant, was sufficient for abrogating the XRCC1 foci formation that was elevated when the canonical OF processing process was inhibited by LIG1 knockdown (Figures 4I, Supplementary Figure S5C).

TIM is necessary for engaging PARP1 to ssDNA gaps behind DNA replication forks

We further sought to determine how TIM promotes the function of PARP1 in the backup OF processing pathway. First, we captured replication fork-associated proteins by the isolation of proteins on nascent DNA (iPOND) to visualize PARP1 localization at active replication forks from HCT116-mAID cells (32). We observed that PARP1 is co-purified with EdU-labeled nascent DNA, which was dramatically increased upon the treatment of FEN1 inhibitor (Figure 5A). Importantly, rapid TIM degradation by 5-Ph-IAA abrogated the increased association of PARP1 and its downstream effector XRCC1 upon FEN1 inhibition, indicating that TIM is necessary for the efficient engagement of PARP1 at active replication forks when the canonical OF processing is impaired. We then reasoned that the PARP1 activity modulated by TIM is specifically located behind DNA replication forks where OF processing and maturation occurs in order for TIM to help engage PARP1 to recognize a series of unprocessed OFs. We therefore determined the localization of PARP1 and XRCC1 by their proximity to EdU-labeled tracts of nascent DNA immediately after pulse labeling and following a chase by thymidine (22). To specifically disrupt the TIM–PARP1 interaction while keeping the replisome intact, we utilized the U2OS DD-PAB-myc cells with Shld1 application. FEN1 inhibition led to a significant increase in the proximal localization of PARP1 to EdU-labeled DNA behind ongoing replication forks, which was abrogated upon Shld1 treatment, suggesting that the TIM–PARP1 interaction is necessary for the proper engagement of PARP1 to ssDNA gaps that accumulate behind ongoing replication forks, presumably at the sites of unligated OF processing (Figures 5B, C). Subsequently, the increased recruitment of XRCC1 to EdU-pulsed and chased nascent DNA was also dependent on the TIM–PARP1 complex (Figures 5D, E). By contrast, the Shld1-stabilized EQ/EQ/TD mutant peptide failed to antagonize the association of PARP1 and XRCC1 to DNA replication forks (Supplementary Figures S5D, S5E). Together, these results underscore the role of the TIM–PARP1 interaction within the replisome in guiding the PARP1 activity required for counteracting the accumulation of OF intermediates and thus ensuring proper lagging strand synthesis.

Disruption of the TIM–PARP1 interaction triggers synergistic replication damage in cells deficient in the canonical OF processing pathway

Thus far, we have demonstrated that the TIM–PARP1 interaction is essential for compensating a defect in the maturation of OF intermediates; we therefore determined whether disruption of both the TIM–PARP1 complex and the canonical OF processing pathway results in synergistic fork instability and cellular lethality. Indeed, while single treatment of 5-Ph-IAA or FEN1 inhibitor in HCT116-mAID-TIM cells did not cause major cytotoxicity, combination of the two led to a severe loss of cellular viability as measured by intracellular ATP levels (Figure 6A). Similarly, their clonogenic survival was impaired in a synergistic manner when TIM was degraded and FEN1 was inhibited (Figures 6B, C). Furthermore, disrupting the interaction between TIM and PARP1 using Shld1 in U2OS DD-PAB-myc WT cells was sufficient to cause a synergistic loss of cellular viability (Figure 6D) and clonogenicity (Figures 6E, F). Mechanistically, we observed a substantial increase of DNA replication damage markers, including pKAP1 S824 and γH2AX, in cells deficient in both TIM and FEN1, indicating that compound ssDNA gap accumulation leads to DNA strand breakage (Figure 6G). Inhibition of the MRE11 nuclease activity by mirin was sufficient for suppressing not only pKAP1 S824, RPA32 S4/S8, and γH2AX levels, but also cleaved PARP1, suggesting that unrepaired ssDNA gaps are expanded by uncontrolled nuclease activities, ultimately becoming a source of genome instability and cell death (Figure 6H). Similar synergistic DNA replication damage was observed when FEN1i and Shld1 were combined in U2OS DD-PAB-myc WT cells (Figure 6I). Taken together, our results define TIM as a synthetic lethal target of OF processing enzymes. The TIM–PARP1 interaction is essential for preventing the catastrophic fork collapse and cell death via supporting the processing of OF intermediates and timely lagging strand synthesis.

Discussion

By implementing both a degron that rapidly degrades endogenous TIM and an inducible polypeptide that disrupts the TIM–PARP1 interaction, we have determined that the TIM–PARP1 complex is an essential element of the DNA replication machinery necessary for efficient DNA replication fork elongation. As a key constituent of the FPC, TIM, together with its obligate heterodimer TIPIN, tethers the CMG helicase and replicative polymerase activities to maintain the integrity of the replisome (2,33,34). Positioning of TIM on dsDNA at the leading edge of CMG stabilizes the replisome and facilitates the separation of leading and lagging strands (3,4). In both yeast and human, TIM augments the function of CLASPIN to stimulate the rate of template unwinding and leading strand progression (6,7). In this study, we show that TIM plays another critical role for DNA replication by helping PARP1 engage a backup OF processing pathway for seamless lagging strand synthesis (Figure 7). Accordingly, rapid TIM loss or disruption of the TIM–PARP1 interaction impairs the PARP1 activity behind DNA replication forks, resulting in an increase of daughter-strand ssDNA gaps and DNA breakage. Its impact is further exacerbated in the absence of LIG1 or FEN1 activity that supports the canonical OF maturation processing, causing synergistic fork instability and loss of cell viability. Insuffi-

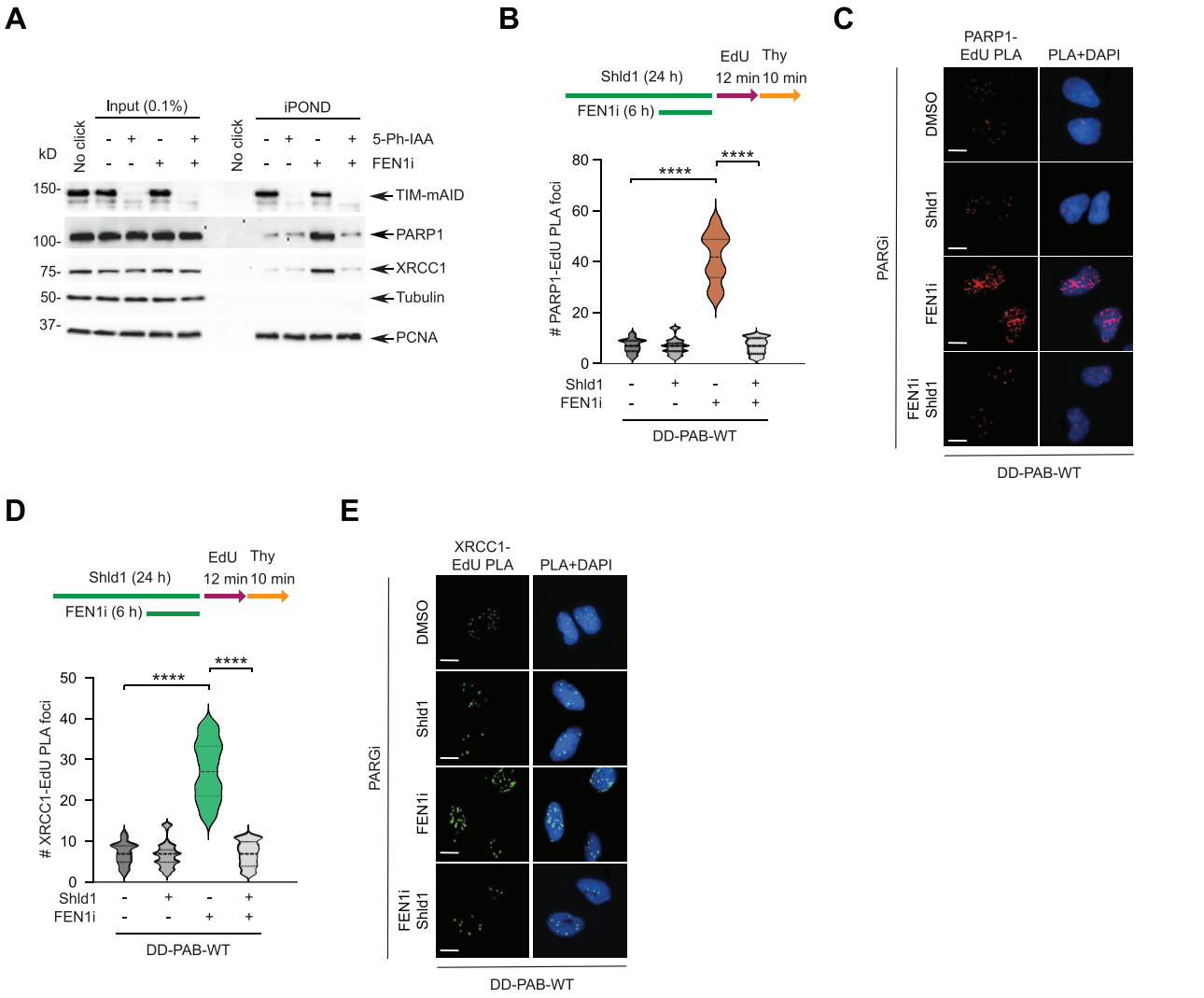

Figure 5. The TIM–PARP1 interaction is necessary for engaging PARP1 to ssDNA gaps behind replication forks. (**A**) HCT116-mAID cells were treated with 10 μM FEN1i for 6 h and/or 1 μM 5-Ph-IAA for 6 h. Following 125 μM EdU pulse and click reaction to conjugate EdU-labeled forks with biotin, replication fork-associated proteins were isolated by iPOND and analyzed by WB. (**B**) Quantification of the numbers of PARP1-EdU PLA foci from cells containing more than two PLA foci. U2OS DD-PAB WT cells were treated with 1 μM Shld1 for 24 h and 10 μM FEN1i for 6 h followed by a brief pulse with 125 μM EdU for 12 min and chase with 1 mM thymidine for another 10 min to label DNA behind replication forks. 10 μM PARGi was treated during the last 20 min of FEN1i incubation and during the EdU pulse. Dashed lines indicate Q1, median, and Q3. $n = 2$, $^{****}P < 0.0001$, Mann–Whitney. (**C**) Representative images of the PARP1-EdU PLA foci. Scale bar: 10 μm. (**D**) Quantification of the numbers of XRCC1-EdU PLA foci. Cells were treated as (B). Dashed lines indicate Q1, median, and Q3. $n = 2$, $^{****}P < 0.0001$, Mann–Whitney. (**E**) Representative images of the XRCC1-EdU PLA foci. Scale bar: 10 μm.

cient PARP1 activity in the absence of TIM will lead to the uncoupling of leading and lagging strand synthesis; asymmetric DNA synthesis is expected to cause frequent fork stalling and ssDNA exposure that will further compromise DNA replication fork stability, which has previously been observed upon Pol α inhibition or in a replication checkpoint-deficient yeast strain (35,36). Therefore, we propose that TIM coordinates the leading and lagging strand synthesis as a scaffold of the replisome to stimulate its activity and as a regulator of PAR-dependent maturation of nascent DNA strands.

Exactly how TIM promotes the action of PARP1 at sites of OF processing is not clear. Given the ability of PARP1 to recognize DNA nicks and ssDNA gaps, PARP1 is expected to gain access to DNA replication forks, however we show that TIM is required for the proper engagement of PARP1 to nascent DNA behind ongoing replication forks. In contrast to the N-terminal rigid α-solenoid helical repeats of TIM that are bound to the MCM subunits, the C-terminus of TIM that mediates its interaction with PARP1 is flexible and not stably positioned within the replisome (3,4). The accommodating nature of the TIM tail region may help PARP1 capture a lagging strand DNA template from a DNA replication fork. A recent cryo-EM structure revealed that the Pol α-primase complex binds directly to the leading edge of CMG in close proximity to TIM, thereby positioning the primase activity right above the exit channel for a lagging strand template (37). This loop-like configuration of a DNA replication fork occupied by the CMG in complex with TIM may allow for the efficient recognition of ssDNA gaps between OF intermediates by PARP1 while TIM enables the flexible tethering of PARP1 to sites of discontinuous DNA replication. The binding interface of PARP1 to the C-terminus of TIM is opposite to the catalytic

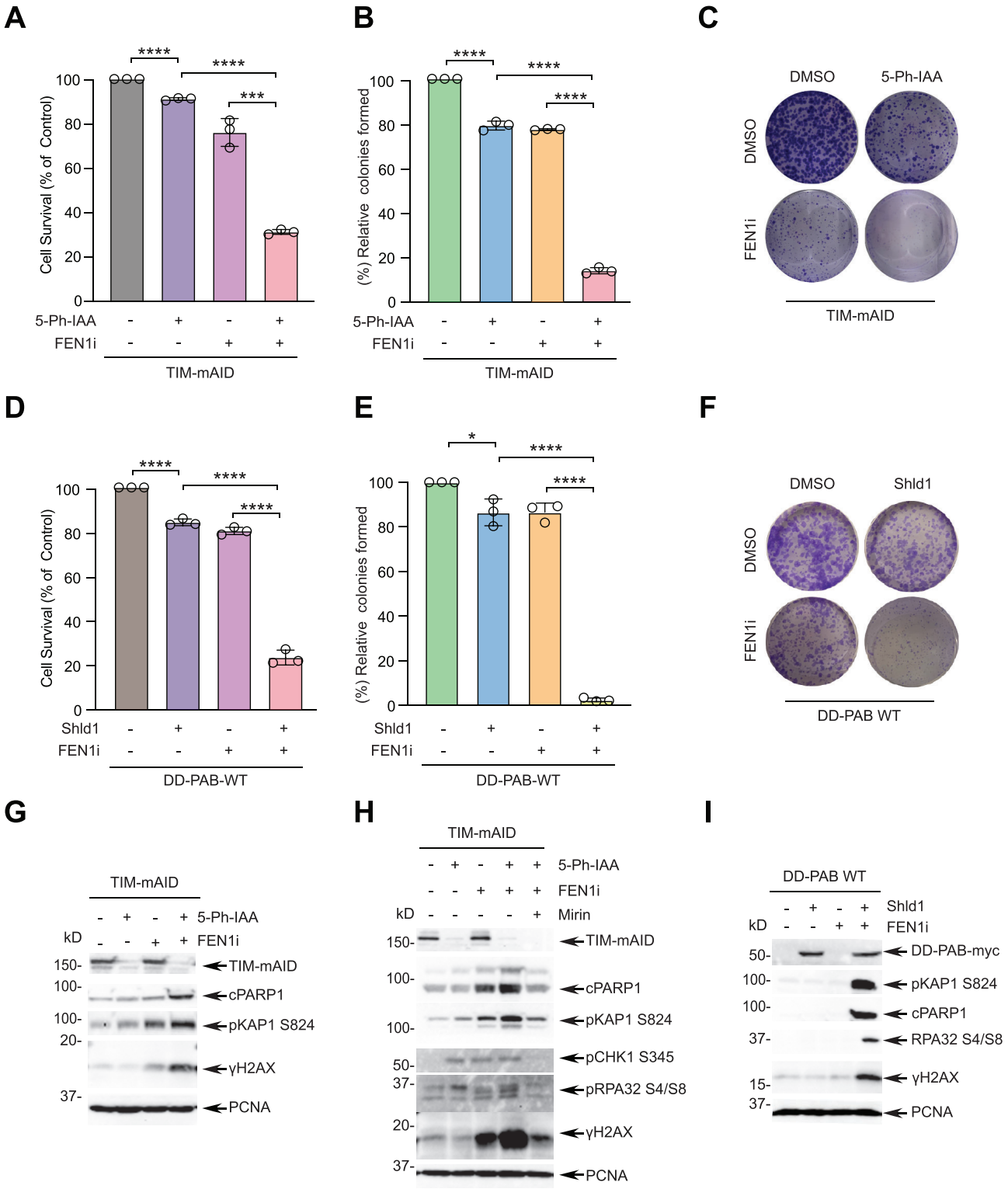

Figure 6. Disruption of the TIM–PARP1 interaction triggers synergistic replication fork instability in cells deficient in the canonical OF processing pathway. (**A**) Quantification of cellular viability measured by ATP-dependent luminescence. TIM-mAID cells were treated with DMSO or 10 μM FEN1i for the first 24 h followed by 1 μM 5-Ph-IAA (versus control) for 3 more days. $n = 3$, mean ± SD, $^{****}P < 0.0001$, $^{***}P < 0.001$, Student's *t*-test. (**B**) Quantification of clonogenic survival of TIM-mAID cells treated with DMSO or 10 μM FEN1i for the first 24 h followed by 1 μM 5-Ph-IAA (versus control) for 11 more days. $n = 3$, mean ± SD, $^{****}P < 0.0001$, Student's *t*-test. (**C**) Representative images of colony formation in (B). (**D**) Quantification of cellular viability measured by ATP-dependent luminescence. U2OS DD-PAB WT cells treated with DMSO or 10 μM FEN1i for the first 24 h followed by 1 μM Shld1 (versus control) for 3 more days. $n = 3$, mean ± SD, $^{****}P < 0.0001$, Student's *t*-test. **(E)** Quantification of clonogenic survival of U2OS DD-PAB WT cells treated with DMSO or 10 μM FEN1i for the first 24 h followed by 1 μM Shld1 (versus control) for 11 more days. $n = 3$, mean ± SD, $^{****}P < 0.0001$, $^{*}P < 0.05$, Student's *t*-test. (**F**) Representative images of colony formation in (E). (**G**) TIM-mAID cells were treated with 1 μM 5-Ph-IAA for 48 h and/or 10 μM FEN1i for the first 24 h, and DNA damage and cell death were analyzed by WB. (**H**) As (G) except where indicated cells were treated with 50 μM mirin for 12 h before harvest. (**I**) U2OS DD-PAB WT cells were first treated with 10 μM FEN1i for 24 h and then replenished with media containing 1 μM Shld1 for additional 48 h. Cell lysates were analyzed by WB.

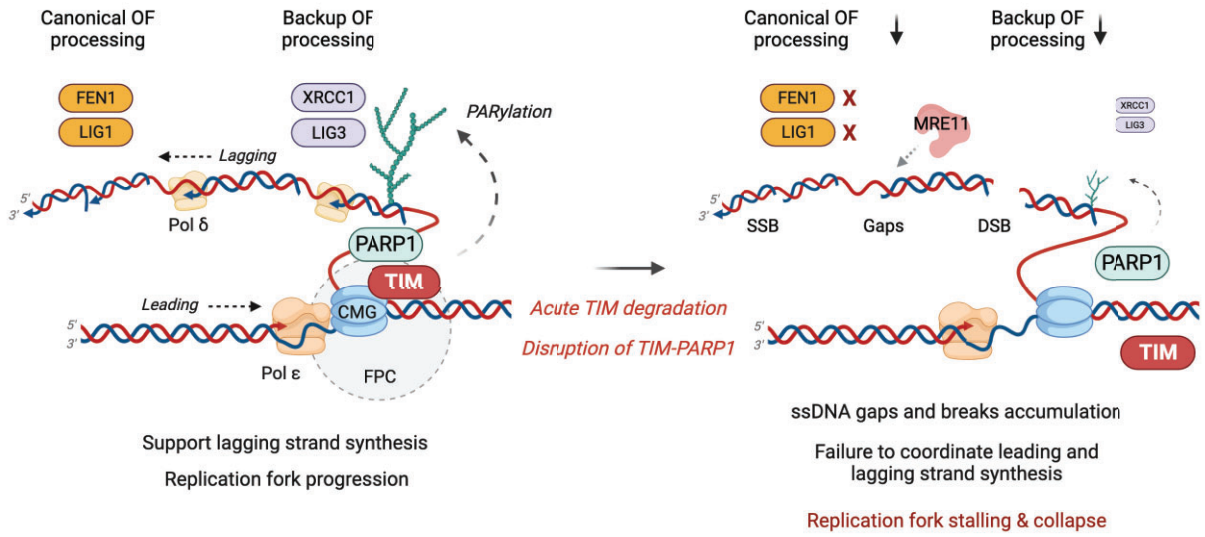

Figure 7. Model depicting the role of TIM in coordinating leading and lagging strand synthesis via PARP1 interaction. As a component of the FPC and scaffold of the replisome, TIM promotes leading strand elongation by ensuring the coupling of the replicative polymerase and CMG helicase activities. TIM directly binds to PARP1 and supports its PARylation necessary for the recruitment of downstream single-strand break repair factors XRCC1 and LIG3, thus promoting the engagement of PARP1 to the backup OF processing pathway when the canonical pathway is evaded. Accordingly, acute TIM degradation or disruption of the TIM–PARP1 interaction results in accumulation of ssDNA gaps and their expansion by nuclease activities, which in the event of a defect in canonical OF processing, leads to synergistic fork instability and cellular lethality associated with DNA replication fork collapse. Image created with Biorender.com.

pocket of PARP1, and TIM does not appear to affect the catalytic activity of PARP1 at least *in vitro* (25). However, we do not exclude the possibility that a local conformational change of PARP1 induced by its interaction with TIM specifically at DNA replication forks may fine-tune PARP1 catalytic activity. PARylation of histone H3 by HPF1-dependent PARP1 activation was shown to support the backup OF processing, and whether TIM controls the association of HPF1 to PARP1 remains to be determined (28). TIM may also regulate proteins at stressed forks, such as TPX2, a newly identified protein that is known to modulate PARP1 activity (38) The sheer number of OF intermediates generated during lagging strand synthesis would require constant action of PARP1 to efficiently recognize ssDNA gaps and recruit downstream SSB repair factors along with the players involved in canonical OF maturation. TIM, via its direct interaction with PARP1, is well-positioned to bring DNA replication and repair together at ongoing replication forks. We thus propose that PARP1 is an essential constituent of the DNA replication machinery supported by the FPC. Notably, TIM only interacts with PARP1, not PARP2 or PARP3 (25), indicating that TIM may have evolved to recognize PARP1-specific sequences to bring the major PAR-conjugating enzyme, PARP1, to the replisome.

Our study uncovers a physiological role of the TIM and PARP1 interaction for the coordination of DNA replication and repair processes, focusing on OF processing. Besides its interaction with the core MCM subunits and CLASPIN as part of the FPC, TIM has been shown to directly interact with quite a few proteins at DNA replication forks, including DDX11, a DNA helicase, and SDE2, a regulatory element that supports TIM stability and localization (12,39,40). Its heterodimeric partner TIPIN is specialized to interact with RPA to propagate the ATR checkpoint response at stalled forks (41). Analogous to monoubiquitinated PCNA, the C-terminus of TIM may act as a docking hub in the replisome, thereby controlling the access of several key genome surveillance proteins at ongoing replication forks. Such plasticity may not only support the processivity of replication fork elongation via MCM interactions, but also help mitigate different DNA replication problems. On the other hand, several proteomics studies reported TIM PARylation under DNA damage (42,43). Indeed, our recent study identified TIM as a substrate of the HPF1-PARP1 complex to be PARylated and demonstrated that PAR-dependent TIM degradation is necessary for stalled fork protection (27). Therefore, an intricate interplay between TIM and PARP1 exists at the replisome to safeguard the integrity of DNA replication forks.

Our work defines the interface of the TIM and PARP1 interaction as a potential therapeutic target for cancer treatment. We devised a way of inducing a TIM polypeptide that can compete with endogenous PARP1 as a proof-of-principle to disrupt the TIM–PARP1 interaction, thereby impeding DNA replication processes and elevating DNA replication stress. We demonstrate that this approach triggers a synthetic lethal interaction with a defect in the canonical OF processing pathway caused by FEN1 inhibition, suggesting that the dysfunctional lagging strand synthesis is incompatible with cell survival. Notably, small-molecule inhibitors targeting FEN1 are being developed for cancer therapy, and identifying small compounds or peptides that can dock to the binding pocket of TIM or PARP1 may allow for a combination therapy that can exacerbate such a replication vulnerability of cancer cells (44,45).

Indeed, cytotoxicity stemming from a problem in lagging strand synthesis has been linked to extensive ssDNA gap accumulation, which underlies the exquisite sensitivity of PARP

inhibition under BRCAness (46). PARP inhibitors produce longer but discontinuous DNA replication tracks, indicating that ssDNA gaps are accumulated without PARP activities (47). At the same time, deficiency in the BRCA1-RAD51 pathway results in PARP1 hyperactivation and renders cells more likely to rely on XRCC1 and LIG3 in the backup OF processing thus supporting the role of BRCA1 in suppressing gap formation (48). 53BP1 counteracts this process; in turn, the loss of LIG3 enhances the cytotoxicity of PARP inhibitors in BRCA1- and 53BP1-deficient cells, suggesting that backup OF processing becomes an acquired determinant of PARP inhibitor sensitivity (48,49). This is distinct from the canonical function of BRCA1 and 53BP1 in controlling DSB repair, and ssDNA gap is therefore considered a better prediction of PARP inhibitor sensitivity. Rather than a mere precursor to fork collapse and DSBs, ssDNA gaps may constitute a unique toxic structure that can be extended and degraded by nucleolytic processing. BRCA1/2 proteins are known to limit the gap processing by MRE11 and promote gap filling (50,51). TIM was shown to protect stalled forks from nucleolytic degradation (12). Whether TIM shares the function of BRCA1/2 in controlling nuclease activities and post-replicative gap repair, including translesion DNA synthesis (TLS), remains uncharacterized. Perhaps, the FPC and the associated PARP1 activity may be involved in the dynamic fate control of DNA replication forks, including PRIMPOL-dependent repriming and fork reversal which are known to modulate the extent of gap induction. It was shown that 53BP1-deficiency decreases TLS-dependent mutagenesis while it restores template switching (TS), a gap filling process at reversed forks, indicating that TS may be associated with gap suppression (52). In this sense, a variety of synthetic lethality exploiting ssDNA gap accumulation during DNA replication is being considered for cancer therapy and has already been applied through the combinatory loss of LIG1 and XRCC1/BRCA2, PARP1 and XRCC1, or PARP1 and ubiquitinated PCNA (51,53,54). Intriguingly, DNA secondary structures that frequently form during DNA replication, such as the G-quadruplex (G4) structure, was shown to resensitize cells with acquired PARP inhibitor resistance through the loss of 53BP1 in BRCA1/2-deficient backgrounds (55). It is thus tempting to speculate that G4-forming ligands may further induce replication-associated gap accumulation on lagging strands by impairing backup OF processing (56), and the unique role of TIM and PARP1 in the resolution of G4s may further contribute to efficient lagging strand synthesis (57,58). Indeed, G4 ligands are being used as a targeted therapeutic agent in cancer (59). A better understanding of the compensatory OF maturation pathway and gap suppression mechanisms will help develop a strategy to target specific determinants of lagging strand synthesis, thus increasing the efficacy of PARP inhibitors and checkpoint inhibitors that destabilize DNA replication forks.

Data availability

All data is available in the main text and supplemental materials. Plasmids and cell lines generated for this study will be made available upon request.

Supplementary data

Supplementary Data are available at NAR Online.

Acknowledgements

We would like to thank Dr Alessandro Vindigni (WashU, USA) for providing the *PRIMOL* knockout cell line, Dr Michael Frohman (Stony Brook University, USA) for providing pcDNA5/FRT/TO and Dr Sharon Cantor (UMass, USA) for helpful suggestions and discussions. Graphical abstract and Figure 7 are created with Biorender.com.

Author contributions: J.S. performed most of the experiments, including generating the U2OS TIM DD-PAB-myc cell lines, and analyzed data. J.R. established the U2OS Flp-In T-REx TIM WT and EQ/EQ/TD cell lines. J.R., A.L.P. N.L. and J.J.P. contributed to the initial characterization of the TIM–PARP1 interaction and siRNA knockdown experiments. J.A.P. established the TIM-mAID degron system and performed some of experiments related to it. H.K. conceptualized and supervised the project, and wrote the manuscript with the assistance of J.S.

Funding

National Institutes of Health [R01GM144399]; American Cancer Society [RSG-18-037-DMC]; Breast Cancer Alliance (to H.K.); National Institutes of Health [F31CA278156 to J.J.P.]; American Cancer Society Institutional Research Grant (to J.R.); J.A.P is a recipient of the Scholars in Biomedical Sciences Fellowship from Renaissance School of Medicine at Stony Brook University. Funding for open access charge: National Institutes of Health [R01GM144399].

Conflict of interest statement

None declared.

References

1. Burgers,P.M.J. and Kunkel,T.A. (2017) Eukaryotic DNA replication fork. *Annu. Rev. Biochem.*, **86**, 417–438.
2. Patel,J.A. and Kim,H. (2023) The TIMELESS effort for timely DNA replication and protection. *Cell. Mol. Life Sci.*, **80**, 84.
3. Baretic,D., Jenkyn-Bedford,M., Aria,V., Cannone,G., Skehel,M. and Yeeles,J.T.P. (2020) Cryo-EM structure of the fork protection complex bound to CMG at a replication fork. *Mol. Cell*, **78**, 926–940.
4. Jones,M.L., Baris,Y., Taylor,M.R.G. and Yeeles,J.T.P. (2021) Structure of a human replisome shows the organisation and interactions of a DNA replication machine. *EMBO J.*, **40**, e108819.
5. Katou,Y., Kanoh,Y., Bando,M., Noguchi,H., Tanaka,H., Ashikari,T., Sugimoto,K. and Shirahige,K. (2003) S-phase checkpoint proteins Tof1 and Mrc1 form a stable replication-pausing complex. *Nature*, **424**, 1078–1083.
6. Baris,Y., Taylor,M.R.G., Aria,V. and Yeeles,J.T.P. (2022) Fast and efficient DNA replication with purified human proteins. *Nature*, **606**, 204–210.
7. Yeeles,J.T.P., Janska,A., Early,A. and Diffley,J.F.X. (2017) How the eukaryotic replisome achieves rapid and efficient DNA replication. *Mol. Cell*, **65**, 105–116.
8. Kilkenny,M.L., Simon,A.C., Mainwaring,J., Wirthensohn,D., Holzer,S. and Pellegrini,L. (2017) The human CTF4-orthologue AND-1 interacts with DNA polymerase alpha/primase via its unique C-terminal HMG box. *Open Biol*, **7**, 170217.
9. Simon,A.C., Zhou,J.C., Perera,R.L., van Deursen,F., Evrin,C., Ivanova,M.E., Kilkenny,M.L., Renault,L., Kjaer,S., Matak-Vinkovic,D., *et al.* (2014) A Ctf4 trimer couples the CMG

helicase to DNA polymerase alpha in the eukaryotic replisome. *Nature*, **510**, 293–297.
10. Kemp,M.G., Akan,Z., Yilmaz,S., Grillo,M., Smith-Roe,S.L., Kang,T.H., Cordeiro-Stone,M., Kaufmann,W.K., Abraham,R.T., Sancar,A., *et al.* (2010) Tipin-replication protein A interaction mediates Chk1 phosphorylation by ATR in response to genotoxic stress. *J. Biol. Chem.*, **285**, 16562–16571.
11. Unsal-Kacmaz,K., Chastain,P.D., Qu,P.P., Minoo,P., Cordeiro-Stone,M., Sancar,A. and Kaufmann,W.K. (2007) The human Tim/Tipin complex coordinates an Intra-S checkpoint response to UV that slows replication fork displacement. *Mol. Cell. Biol.*, **27**, 3131–3142.
12. Rageul,J., Park,J.J., Zeng,P.P., Lee,E.A., Yang,J., Hwang,S., Lo,N., Weinheimer,A.S., Scharer,O.D., Yeo,J.E., *et al.* (2020) SDE2 integrates into the TIMELESS-TIPIN complex to protect stalled replication forks. *Nat. Commun.*, **11**, 5495.
13. Ogawa,T. and Okazaki,T. (1980) Discontinuous DNA replication. *Annu. Rev. Biochem.*, **49**, 421–457.
14. Zheng,L. and Shen,B. (2011) Okazaki fragment maturation: nucleases take centre stage. *J. Mol. Cell Biol.*, **3**, 23–30.
15. Stodola,J.L. and Burgers,P.M. (2017) Mechanism of lagging-strand DNA replication in eukaryotes. *Adv. Exp. Med. Biol.*, **1042**, 117–133.
16. Ray Chaudhuri,A. and Nussenzweig,A. (2017) The multifaceted roles of PARP1 in DNA repair and chromatin remodelling. *Nat. Rev. Mol. Cell Biol.*, **18**, 610–621.
17. O'Sullivan,J., Tedim Ferreira,M., Gagne,J.P., Sharma,A.K., Hendzel,M.J., Masson,J.Y. and Poirier,G.G. (2019) Emerging roles of eraser enzymes in the dynamic control of protein ADP-ribosylation. *Nat. Commun.*, **10**, 1182.
18. Hanzlikova,H., Kalasova,I., Demin,A.A., Pennicott,L.E., Cihlarova,Z. and Caldecott,K.W. (2018) The importance of poly(ADP-ribose) polymerase as a sensor of unligated Okazaki fragments during DNA replication. *Mol. Cell*, **71**, 319–331.
19. Arakawa,H. and Iliakis,G. (2015) Alternative Okazaki fragment ligation pathway by DNA ligase III. *Genes (Basel)*, **6**, 385–398.
20. Breslin,C., Hornyak,P., Ridley,A., Rulten,S.L., Hanzlikova,H., Oliver,A.W. and Caldecott,K.W. (2015) The XRCC1 phosphate-binding pocket binds poly (ADP-ribose) and is required for XRCC1 function. *Nucleic Acids Res.*, **43**, 6934–6944.
21. Caldecott,K.W., McKeown,C.K., Tucker,J.D., Ljungquist,S. and Thompson,L.H. (1994) An interaction between the mammalian DNA repair protein XRCC1 and DNA ligase III. *Mol. Cell. Biol.*, **14**, 68–76.
22. Vaitsiankova,A., Burdova,K., Sobol,M., Gautam,A., Benada,O., Hanzlikova,H. and Caldecott,K.W. (2022) PARP inhibition impedes the maturation of nascent DNA strands during DNA replication. *Nat. Struct. Mol. Biol.*, **29**, 329–338.
23. Patel,J.A., Zezelic,C., Rageul,J., Saldanha,J., Khan,A. and Kim,H. (2023) Replisome dysfunction upon inducible TIMELESS degradation synergizes with ATR inhibition to trigger replication catastrophe. *Nucleic Acids Res.*, **51**, 6246–6263.
24. Quinet,A., Carvajal-Maldonado,D., Lemacon,D. and Vindigni,A. (2017) DNA fiber analysis: mind the gap!. *Methods Enzymol.*, **591**, 55–82.
25. Xie,S., Mortusewicz,O., Ma,H.T., Herr,P., Poon,R.Y., Helleday,T. and Qian,C. (2015) Timeless interacts with PARP-1 to promote homologous recombination repair. *Mol. Cell*, **60**, 163–176.
26. Young,L.M., Marzio,A., Perez-Duran,P., Reid,D.A., Meredith,D.N., Roberti,D., Star,A., Rothenberg,E., Ueberheide,B. and Pagano,M. (2015) TIMELESS forms a complex with PARP1 distinct from its complex with TIPIN and plays a role in the DNA damage response. *Cell Rep.*, **13**, 451–459.
27. Rageul,J., Lo,N., Phi,A.L., Patel,J.A., Park,J.J. and Kim,H. (2024) Poly(ADP-ribosyl)ation of TIMELESS limits DNA replication stress and promotes stalled fork protection. *Cell Rep.*, **43**, 113845.
28. Kumamoto,S., Nishiyama,A., Chiba,Y., Miyashita,R., Konishi,C., Azuma,Y. and Nakanishi,M. (2021) HPF1-dependent PARP activation promotes LIG3-XRCC1-mediated backup pathway of Okazaki fragment ligation. *Nucleic Acids Res.*, **49**, 5003–5016.
29. Caldecott,K.W., Aoufouchi,S., Johnson,P. and Shall,S. (1996) XRCC1 polypeptide interacts with DNA polymerase beta and possibly poly (ADP-ribose) polymerase, and DNA ligase III is a novel molecular 'nick-sensor' in vitro. *Nucleic Acids Res.*, **24**, 4387–4394.
30. El-Khamisy,S.F., Masutani,M., Suzuki,H. and Caldecott,K.W. (2003) A requirement for PARP-1 for the assembly or stability of XRCC1 nuclear foci at sites of oxidative DNA damage. *Nucleic Acids Res.*, **31**, 5526–5533.
31. Banaszynski,L.A., Chen,L.C., Maynard-Smith,L.A., Ooi,A.G. and Wandless,T.J. (2006) A rapid, reversible, and tunable method to regulate protein function in living cells using synthetic small molecules. *Cell*, **126**, 995–1004.
32. Sirbu,B.M., Couch,F.B. and Cortez,D. (2012) Monitoring the spatiotemporal dynamics of proteins at replication forks and in assembled chromatin using isolation of proteins on nascent DNA. *Nat. Protoc.*, **7**, 594–605.
33. Leman,A.R. and Noguchi,E. (2012) Local and global functions of Timeless and Tipin in replication fork protection. *Cell Cycle*, **11**, 3945–3955.
34. Chou,D.M. and Elledge,S.J. (2006) Tipin and Timeless form a mutually protective complex required for genotoxic stress resistance and checkpoint function. *Proc. Natl. Acad. Sci. U.S.A.*, **103**, 18143–18147.
35. Ercilla,A., Benada,J., Amitash,S., Zonderland,G., Baldi,G., Somyajit,K., Ochs,F., Costanzo,V., Lukas,J. and Toledo,L. (2020) Physiological tolerance to ssDNA enables strand uncoupling during DNA replication. *Cell Rep.*, **30**, 2416–2429.
36. Serra-Cardona,A., Yu,C., Zhang,X., Hua,X., Yao,Y., Zhou,J., Gan,H. and Zhang,Z. (2021) A mechanism for Rad53 to couple leading- and lagging-strand DNA synthesis under replication stress in budding yeast. *Proc. Natl. Acad. Sci. U.S.A.*, **118**, e2109334118.
37. Jones,M.L., Aria,V., Baris,Y. and Yeeles,J.T.P. (2023) How Pol alpha-primase is targeted to replisomes to prime eukaryotic DNA replication. *Mol. Cell*, **83**, 2911–2924.
38. Mosler,T., Baymaz,H.I., Graf,J.F., Mikicic,I., Blattner,G., Bartlett,E., Ostermaier,M., Piccinno,R., Yang,J., Voigt,A., *et al.* (2022) PARP1 proximity proteomics reveals interaction partners at stressed replication forks. *Nucleic Acids Res.*, **50**, 11600–11618.
39. Cali,F., Bharti,S.K., Di Perna,R., Brosh,R.M. Jr and Pisani,F.M. (2016) Tim/Timeless, a member of the replication fork protection complex, operates with the Warsaw breakage syndrome DNA helicase DDX11 in the same fork recovery pathway. *Nucleic Acids Res.*, **44**, 705–717.
40. Weinheimer,A.S., Paung,Y., Rageul,J., Khan,A., Lo,N., Ho,B., Tong,M., Alphonse,S., Seeliger,M.A. and Kim,H. (2022) Extended DNA-binding interfaces beyond the canonical SAP domain contribute to the function of replication stress regulator SDE2 at DNA replication forks. *J. Biol. Chem.*, **298**, 102268.
41. Saldanha,J., Rageul,J., Patel,J.A. and Kim,H. (2023) The adaptive mechanisms and checkpoint responses to a stressed DNA replication fork. *Int. J. Mol. Sci.*, **24**, 10488.
42. Hendriks,I.A., Buch-Larsen,S.C., Prokhorova,E., Elsborg,J.D., Rebak,A., Zhu,K., Ahel,D., Lukas,C., Ahel,I. and Nielsen,M.L. (2021) The regulatory landscape of the human HPF1- and ARH3-dependent ADP-ribosylome. *Nat. Commun.*, **12**, 5893.
43. Hendriks,I.A., Larsen,S.C. and Nielsen,M.L. (2019) An advanced strategy for comprehensive profiling of ADP-ribosylation sites using mass spectrometry-based proteomics. *Mol. Cell. Proteomics*, **18**, 1010–1026.
44. Guo,E., Ishii,Y., Mueller,J., Srivatsan,A., Gahman,T., Putnam,C.D., Wang,J.Y.J. and Kolodner,R.D. (2020) FEN1 endonuclease as a therapeutic target for human cancers with defects in homologous recombination. *Proc. Natl. Acad. Sci. U.S.A.*, **117**, 19415–19424.
45. Yang,F., Hu,Z. and Guo,Z. (2022) Small-molecule inhibitors targeting FEN1 for cancer therapy. *Biomolecules*, **12**.

46. Cantor,S.B. (2021) Revisiting the BRCA-pathway through the lens of replication gap suppression: "Gaps determine therapy response in BRCA mutant cancer". *DNA Repair (Amst.)*, **107**, 103209.
47. Maya-Mendoza,A., Moudry,P., Merchut-Maya,J.M., Lee,M., Strauss,R. and Bartek,J. (2018) High speed of fork progression induces DNA replication stress and genomic instability. *Nature*, **559**, 279–284.
48. Cong,K., Peng,M., Kousholt,A.N., Lee,W.T.C., Lee,S., Nayak,S., Krais,J., VanderVere-Carozza,P.S., Pawelczak,K.S., Calvo,J., *et al.* (2021) Replication gaps are a key determinant of PARP inhibitor synthetic lethality with BRCA deficiency. *Mol. Cell*, **81**, 3128–3144.
49. Paes Dias,M., Tripathi,V., van der Heijden,I., Cong,K., Manolika,E.M., Bhin,J., Gogola,E., Galanos,P., Annunziato,S., Lieftink,C., *et al.* (2021) Loss of nuclear DNA ligase III reverts PARP inhibitor resistance in BRCA1/53BP1 double-deficient cells by exposing ssDNA gaps. *Mol. Cell*, **81**, 4692–4708.
50. Quinet,A., Tirman,S., Jackson,J., Svikovic,S., Lemacon,D., Carvajal-Maldonado,D., Gonzalez-Acosta,D., Vessoni,A.T., Cybulla,E., Wood,M., *et al.* (2020) PRIMPOL-mediated adaptive response suppresses replication fork reversal in BRCA-deficient cells. *Mol. Cell*, **77**, 461–474.
51. Tirman,S., Quinet,A., Wood,M., Meroni,A., Cybulla,E., Jackson,J., Pegoraro,S., Simoneau,A., Zou,L. and Vindigni,A. (2021) Temporally distinct post-replicative repair mechanisms fill PRIMPOL-dependent ssDNA gaps in human cells. *Mol. Cell*, **81**, 4026–4040.
52. Chen,D., Gervai,J.Z., Poti,A., Nemeth,E., Szeltner,Z., Szikriszt,B., Gyure,Z., Zamborszky,J., Ceccon,M., d'Adda di Fagagna,F., *et al.* (2022) BRCA1 deficiency specific base substitution mutagenesis is dependent on translesion synthesis and regulated by 53BP1. *Nat. Commun.*, **13**, 226.
53. Strom,C.E., Johansson,F., Uhlen,M., Szigyarto,C.A., Erixon,K. and Helleday,T. (2011) Poly (ADP-ribose) polymerase (PARP) is not involved in base excision repair but PARP inhibition traps a single-strand intermediate. *Nucleic Acids Res.*, **39**, 3166–3175.
54. Thakar,T., Leung,W., Nicolae,C.M., Clements,K.E., Shen,B., Bielinsky,A.K. and Moldovan,G.L. (2020) Ubiquitinated-PCNA protects replication forks from DNA2-mediated degradation by regulating Okazaki fragment maturation and chromatin assembly. *Nat. Commun.*, **11**, 2147.
55. Zimmer,J., Tacconi,E.M.C., Folio,C., Badie,S., Porru,M., Klare,K., Tumiati,M., Markkanen,E., Halder,S., Ryan,A., *et al.* (2016) Targeting BRCA1 and BRCA2 deficiencies with G-quadruplex-interacting compounds. *Mol. Cell*, **61**, 449–460.
56. van Schendel,R., Romeijn,R., Buijs,H. and Tijsterman,M. (2021) Preservation of lagging strand integrity at sites of stalled replication by Pol alpha-primase and 9-1-1 complex. *Sci. Adv.*, **7**, eabf2278.
57. Lerner,L.K., Holzer,S., Kilkenny,M.L., Svikovic,S., Murat,P., Schiavone,D., Eldridge,C.B., Bittleston,A., Maman,J.D., Branzei,D., *et al.* (2020) Timeless couples G-quadruplex detection with processing by DDX11 helicase during DNA replication. *EMBO J.*, **39**, e104185.
58. Edwards,A.D., Marecki,J.C., Byrd,A.K., Gao,J. and Raney,K.D. (2021) G-Quadruplex loops regulate PARP-1 enzymatic activation. *Nucleic Acids Res.*, **49**, 416–431.
59. Kosiol,N., Juranek,S., Brossart,P., Heine,A. and Paeschke,K. (2021) G-quadruplexes: a promising target for cancer therapy. *Mol. Cancer*, **20**, 40.

Received: January 3, 2024. **Revised:** April 9, 2024. **Editorial Decision:** May 2, 2024. **Accepted:** May 10, 2024